NASA/TP-1998-208465

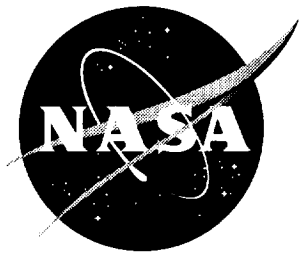

High-Alpha Research Vehicle Lateral-Directional Control Law Description, Analyses, and Simulation Results

John B. Davidson, Patrick C. Murphy, and Frederick J. Lallman
Langley Research Center, Hampton, Virginia

Keith D. Hoffler
ViGYAN, Inc., Hampton, Virginia

Barton J. Bacon
Langley Research Center, Hampton, Virginia

National Aeronautics and
Space Administration

Langley Research Center
Hampton, Virginia 23681-2199

October 1998

Acknowledgments

The authors wish to acknowledge the following individuals who made important contributions to this work:

NASA Langley test pilots Philip Brown, Michael Phillips, and Robert Rivers provided flying qualities ratings and insightful comments for the piloted simulation tasks.

Michael Messina, Lockheed Engineering and Sciences Corporation, maintained the nonlinear batch simulation and provided numerous linear design models.

Susan Carzoo, Unisys Corporation, maintained the real time software for the piloted simulation.

Jim Duricy, Vince Innanaci, Eric Johnson, John Gloystein, Mike Tison, and Brian Gallo, George Washington University graduate students, programmed and tested algorithms used for control law performance and robustness analysis and parameter identification.

Available from:

NASA Center for AeroSpace Information (CASI)
7121 Standard Drive
Hanover, MD 21076-1320
(301) 621-0390

National Technical Information Service (NTIS)
5285 Port Royal Road
Springfield, VA 22161-2171
(703) 605-6000

SUMMARY

This report contains a description of a lateral-directional control law designed for the NASA High-Alpha Research Vehicle (HARV). The HARV is a modified McDonnell-Douglas F/A-18 that began flight evaluation in mid-calendar year 1991. The main modification for the initial phase of this program was the addition of a research flight computer, spin chute, and thrust-vectored controls in the pitch and yaw axes. After initial evaluation flights were completed, revised control laws (designated NASA-1A) were installed on the HARV. Two separate design tools, CRAFT and Pseudo Controls, were integrated to synthesize the revised lateral-directional control law. This report contains a description of this lateral-directional control law, analyses, and nonlinear simulation (batch and piloted) results. Linear analysis results include closed-loop eigenvalues, stability margins, robustness to changes in various plant parameters, and servo-elastic frequency responses. Step time responses from nonlinear batch simulation are presented and compared to design guidelines. Piloted simulation task scenarios, task guidelines, and pilot subjective ratings for the various maneuvers are discussed. Linear analysis shows that the control law meets the stability margin guidelines and is robust to stability and control parameter changes. Nonlinear batch simulation analysis shows the control law exhibits good performance and meets most of the design guidelines over the entire range of angle of attack. The control law was extensively exercised in piloted simulation and shown to possess good flying qualities and to be very departure resistant. This control law was flight tested during the Summer of 1994 at NASA Dryden Flight Research Center.

INTRODUCTION

Advances in weapons and aircraft technology are significantly changing air combat. In the past, air combat engagements often resulted in tail-chase fights measured in minutes; now they are measured in seconds with combatants using all-aspect weapons. Future fighters may have to operate in environments where enhanced maneuverability and controllability throughout a greatly expanded flight envelope, including high angle of attack, are requirements. Studies involving piloted and numerical air combat simulations (Herbst and Krogull 1972; Herbst 1980; Hamilton and Skow 1984; Ogburn et al. 1988; Doane et al. 1990; Fears et al. 1997) have shown that fighters with this capability are able to perform combat maneuvers in shorter time and in less space and thus achieve a tactical advantage. New control effectors, such as thrust-vectoring and actuated nose strakes, offer the capability to expand the flight envelope with greater control than previously obtainable. Success in the fighter combat arena of the future will demand increased capability from aircraft technology.

As part of NASA's High Alpha Technology Program (HATP), key high angle of attack technologies were demonstrated on the High-Alpha Research Vehicle (HARV). One such technology is advanced control concepts including thrust-vectoring and advanced aerodynamic controls. The HARV is a modified McDonnell-Douglas F/A-18 that began flight evaluation in mid-calendar year 1991. The main aircraft modification for the initial phase of this program was the addition of a research flight computer, spin chute and thrust-vectoring in the pitch and yaw axes; resulting in an aircraft that is approximately 4 100 pounds heavier than an unmodified F/A-18. The HARV is designed to operate at angles of attack up to 70 degrees. The original thrust-vectoring control laws, developed jointly by NASA and McDonnell Aircraft Company, were used during the initial high angle-of-attack HARV flight evaluations that included flight envelope expansion and maneuvering capability. Revised control laws that use advanced control design methodologies (Davidson et al. 1992; Ostroff et al. 1994) were then installed on the HARV (after the initial evaluation flights were completed). Initial versions of these control laws (designated NASA-1A) were flight tested during the Summer of 1994 at NASA Dryden Flight Research Center. This report describes the NASA-1A lateral-directional control law.

This report contains a description of the lateral-directional control law, results of analyses, and nonlinear simulation (batch and piloted) results. Linear analysis results include closed-loop eigenvalues, stability margins, robustness to changes in various plant parameters, and servo-elastic frequency responses. Batch simulation results include step-input time responses at selected design conditions and a comparison of

performance with design guidelines (Hoffler et al. 1994). Task scenarios, task guidelines, and Cooper-Harper Ratings (Cooper and Harper 1969) for the various maneuvers are presented in the piloted simulation section. The final section presents concluding remarks.

NOMENCLATURE

A	Plant matrix
A_s	Commanded Accelerations
B	Control distribution matrix for states
Bdot	Sideslip rate
C	State distribution matrix for outputs
D	Control distribution matrix for outputs
G	Feedback gain matrix
G_{fl}	Pseudo control blending matrix
L_{avail}	Roll moment available from controls
L_p	Roll moment due to roll rate
L_{ail}	Roll moment due to aileron
$L_{\delta stab}$	Roll moment due to differential stabilator
l	Number of measurements
λ_i	Eigenvalue for mode *i*
M	State distribution matrix for measurements
m	Number of controls
N	Control distribution matrix for measurements
N_{avail}	Yaw moment available from controls
N_v	Yaw moment due to lateral velocity
N_r	Yaw moment due to yaw rate
N_{rud}	Yaw moment due to rudder
N_{yjet}	Yaw moment due to thrust-vectoring
N_z	Normal acceleration
N_y	Lateral acceleration
n	Number of states
P	Roll rate
Q	Pitch rate
R	Yaw rate
s	Laplace variable, s=jω
$^t\Delta\phi_{w=90}$	Time to bank through a bank angle change of 90 degrees
V_0	Trim velocity
Vroll	Lateral Pseudo Control
Vyaw	Directional Pseudo Control
Y_v	Side Force due to lateral velocity
x	State vector

z	Measurement vector
α	Angle of attack
β	Sideslip
Δ	Uncertainty model
δ	Input vector
ϕ	Bank angle
μ_R^{-1}	Minimum inverse real structured singular value
ω	Frequency
ζ	Damping ratio

Subscripts:

body	body-axis
cmd	commanded
dir	directional axis
dr	dutch roll
lat	lateral axis
n	structural filtered
os	overshoot
pilot	pilot
roll	roll mode
sprl	spiral mode
stab	stability-axis
t	total (rigid body plus flexible modes)
z	measurement

Abbreviations:

A/B	Afterburner
ACM	Air Combat Maneuvering
AOA	Angle Of Attack
CHR	Cooper-Harper Rating
CRAFT	Control power, Robustness, Agility, Flying qualities Trade-offs
DEA	Direct Eigenspace Assignment
DMS	Differential Maneuvering Simulator
HARV	High-Alpha Research Vehicle
HATP	High-Alpha Technology Program
HUD	Head-Up Display
PIO	Pilot Induced Oscillation
RFCS	Research Flight Control System
TV	Thrust-Vectoring

DESCRIPTION OF FACILITIES

Aircraft Configuration

The configuration used for this design is a F/A-18 modified to have multi-axis thrust-vectoring for additional pitch and yaw control power. This modified F/A-18 is referred to as the High-Alpha Research Vehicle (HARV) (Figure 1) and is discussed in more detail in Gilbert and Gatlin 1990. The F/A-18 is a twin engine, single-place, fighter/attack airplane with (by today's standards) good low-speed, high angle-of-attack maneuvering capability. It is powered by two modified General Electric F404-GE-400 afterburning turbofan engines, each rated at approximately 16 000 pounds static thrust at sea level. The HARV has five conventional aerodynamic control surfaces - stabilators, rudders, ailerons, leading-edge flaps, and trailing-edge flaps. Maximum control surface position and rate limits are presented in Table 1. Thrust-vectoring capability has been added to the basic F/A-18 aircraft by removing the divergent flap portion of the engine nozzles and adding externally mounted engine thrust vanes (three for each engine) for deflection of the exhaust plume. Major dimensions and features of the HARV are shown in Figure 2.

The HARV is approximately 4 100 pounds heavier than an F/A-18. The weight of the thrust-vectoring system (approximately 2 200 pounds), spin chute, emergency systems, and ballast is approximately 3 700 pounds. The remaining weight is due to equipment and wiring not directly associated with the thrust-vectoring system. A comparison of the physical characteristics of a F/A-18 and the HARV is presented in Table 2.

A Research Flight Control System (RFCS) consisting of a new longitudinal control law (Ostroff and Profitt 1993; Ostroff et al. 1994) and the lateral-directional control law discussed herein replaced the existing F/A-18 control system. The thrust-vectoring commands from the RFCS go to a vane control system known as the Mixer/Predictor (Bundick et al. 1996). The Mixer/Predictor converts pitch, yaw, and roll thrust-vectoring commands into equivalent commands for the six thrust-vectoring vanes to yield the required jet plume deflection.

Batch Simulation

The HARV nonlinear batch simulation was built from nonlinear aerodynamic, engine, and control system models of the production F/A-18 obtained from McDonnell-Douglas Aerospace (MDA). The original MDA aerodynamic data base covers the angle of attack range from −10 to 90 degrees, the sideslip range from −20 to 20 degrees, altitudes up to 60 000 feet, and speeds up to Mach 2.0. Aerodynamic increments were added to the database to account for the addition of thrust-vectoring vanes, actuator housings, and spin chute. Jet induced effects were added to account for the change in airflow over the airframe due to thrust-vectoring (Bowers et al. 1990).

The engine model incorporated thrust-vectoring capability and included the effects of Mach, altitude, and the dynamic response of engine thrust. Also included were the effects of angle of attack and vane deflection on thrust. Gross thrust and ram drag were tabulated separately allowing thrust-vectoring to act on gross thrust only.

The simulation nominally used the HARV weight and inertias with 60% internal fuel. Heavy (maximum fuel) and light (minimum fuel) conditions were also evaluated; however only results from the nominal configuration are shown in this report. Weights, inertias, and center-of-gravity locations for all three weight conditions are shown in Table 3. The F/A-18 simulation on which the HARV model is based is discussed in detail in Buttrill et al. 1992, and the HARV thrust-vectoring capabilities are discussed in Mason et al. 1992.

Piloted Simulation Facilities

The piloted portion of the control law design effort was conducted using the NASA Langley Differential Maneuvering Simulator (DMS). The DMS is a fixed-base simulator that has the capability of simulating two airplanes as they maneuver relative to each other and the Earth. A wide-angle visual display is provided for each pilot. The general arrangement of the DMS hardware is shown in Figure 3. The DMS consists of two forty-foot diameter projection spheres each enclosing a cockpit, airplane image projection system, and Computer Generated Image (CGI) sky-Earth-sun projection system. Each pilot is provided a projected image of his opponent's airplane, giving range and attitude cues. A detailed (but not current) description of the DMS is given in Ashworth and Kahlbaum 1973.

The DMS is driven by a real-time digital simulation system built around a CONVEX 3800 computer. The dynamics of the airplane and control system were calculated by using six-degree-of-freedom rigid-body equations of motion with an 80 Hz frame rate. Data communication between the computers and the simulation hardware were conducted at a 40 Hz frame rate. Overall transport delay between the cockpit controls and the visual scene display is approximately 110 milliseconds.

A photograph of one of the cockpits and target visual display is shown in Figure 4. Each cockpit incorporates three Cathode Ray Tube (CRT) head-down displays and a Head-Up Display (HUD) with a computer-driven gunsight representative of current fighter aircraft equipment. For this study, a fixed reticle projected on the HUD was used for tracking. The displays provided to the pilot are similar to standard F/A-18 displays with some minor modifications to facilitate some of the test maneuvers and tracking tasks.

A movable center stick was provided for pitch and roll commands from the pilot. Longitudinal and lateral stick forces and gradients were configured to model those of the F/A-18. Longitudinal stick travel was 2.5 inches forward and 5 inches aft with a force gradient of seven pounds per inch and a two pound breakout force. Lateral stick travel was ±3 inches with a force gradient of three pounds per inch and a two pound breakout force. The pedal travel was ±1 inch with a force gradient of 100 pounds per inch and no breakout force.

CONTROL LAW DESIGN

Design Methods

Two separate design tools, CRAFT (Murphy and Davidson 1991) and Pseudo Controls (Lallman 1985), were integrated to synthesize the lateral-directional control law. This combined CRAFT/Pseudo Controls design approach is a hybrid technique that combines both linear and nonlinear design methods.

Pseudo Controls Method

The purpose of Pseudo Controls is to coordinate a number of physical controls in order to provide independent channels of control of aircraft motions. The Pseudo Controls method results in algorithms to organize the aerodynamic and thrust-vectoring control activity so that rolling commands cause body-axis rolling moments with a minimum of yawing moment and yawing commands cause body-axis yawing moments with a minimum of body-axis rolling moments (See Figure 5). A benefit of this technique is that the feedback controller is required to generate fewer outputs (commands), and thus the number of feedback gains is reduced.

For the HARV, the three primary aerodynamic controls used for lateral-directional control are: ailerons that are deflected differentially, twin rudders that are deflected collectively, and horizontal stabilators that are deflected differentially. These controls produce varying amounts of rolling moment, yawing moment, and sideforce depending on flight condition (especially dynamic pressure and angle of attack). The thrust-vectoring apparatus produces control moments that are proportional to the vane deflection angles and the

thrust of the engines. The Pseudo Controls method organizes the aerodynamic and thrust-vectoring control activity to cause moments about the airplane axes that satisfy the demands of stability augmentation feedback loops, pilot commands, and inertial decoupling.

In the HARV design, the Pseudo Controls method converts stability-axis angular acceleration commands into coordinated control deflections. The acceleration commands are distributed to the physical control effectors in proportions that are scheduled according to flight condition. Automatic engagement of the thrust-vectoring controls is based on calculations of their control moment producing capabilities relative to that of the aerodynamic controls. When engaged, the thrust-vectoring controls are driven in proportion to the aerodynamic controls with the magnitudes of the conventional control deflections adjusted to account for the increased control power. Because of concern about possible over-heating of the thrust turning vanes, steady-state thrust-vectoring commands are replaced by increased deflections of aerodynamic controls where possible.

An early development of the Pseudo Controls methodology can be found in Lallman 1985, and its application to the lateral-directional control of the HARV can be found in Lallman et al. 1998.

CRAFT Design Method

The design method used to synthesize feedback gains is referred to as CRAFT which stands for the design objectives addressed, namely, Control power, Robustness, Agility, and Flying Qualities Tradeoffs (Figure 6). This method provides the designer with a graphical tool to simultaneously assess metrics from the four design objective areas. The strength of this approach comes from the use of eigenspace assignment (Srinathkumar 1978), which allows direct specification of eigenvalues and eigenvectors in the design, in combination with graphical overlays of metric surfaces which capture the design goals in a composite illustration on the design space. In this approach, design tradeoffs are made by interpreting graphical overlays of metric surfaces that quantitatively characterize each design goal. Numerous metrics can be applied simultaneously from each of the four design objective areas or any area for which metrics can be expressed in engineering terms. Graphical overlays of the metric surfaces show the best design compromise for all the design criteria and display the "cost" of changing from that design point. This can greatly enhance the designer's ability to make informed design tradeoffs.

CRAFT is summarized in block diagram form in Figure 7. The design process begins by selecting, as the design space, a reasonable range of frequency and damping for the closed-loop dynamics of interest. Within this range, a grid of design points is chosen to systematically cover the design space. Some metrics may be known before the closed-loop design, such as flying qualities specifications. However, the control power, robustness, and agility metrics require determination of the closed-loop system. Using Direct Eigenspace Assignment (DEA) (Davidson and Schmidt 1986) as the control design algorithm, feedback gains are computed to achieve the desired placement of the eigenvalues for the closed-loop system at each design point. With eigenspace assignment, the designer also must define eigenvectors; eigenvectors are chosen to shape the system response or provide modal decoupling.

Once the desired closed-loop systems are determined for a desired set of frequency (ω) and damping (ζ) pairs, each control design metric can be evaluated and plotted producing a surface over the ζ-ω design space. Viewing the metric surface in a 2-dimensional contour plot highlights the most desirable region to locate the closed-loop pole with respect to the particular metric studied. The individual metric surfaces are an indication of the sensitivity of that metric to closed-loop pole location. A final overlay plot of desirable regions from each metric surface can then be obtained. This is represented by the second block from the right in Figure 7. The intersection of desirable regions provide the best design compromise for all the design criteria considered. Often desirable regions may not overlap and some compromise will be required.

Further details of the method and control design metrics can be found in Murphy and Davidson 1991, and its application to the HARV can be found in Murphy and Davidson 1998.

CRAFT Design Metrics

The flying qualities criteria used to design the lateral-directional control law are drawn from several sources. For low angle of attack, the Mil-STD 1797A (Aeronautical Systems Division 1990) and the fighter-specific study of Moorhouse and Moran 1985 were used. For high angle of attack, virtually no information was available to define flying qualities specifications at the beginning of this effort. Consequently, NASA sponsored McDonnell Douglas Aerospace (MDA) to develop longitudinal and lateral flying qualities criteria (Wilson et al. 1993b) using fixed-based simulation at 30, 45, and 60 degrees angle of attack. A generic fighter aircraft model was used during the simulations, and a wide range of closed-loop responses were evaluated. These criteria, presented in both low-order equivalent system modal parameter and Bode envelope formats, are summarized in Wilson and Citurs 1996.

The metric chosen to characterize control power is based on a Euclidean norm of feedback gains and indirectly represents a measure of control power required to achieve each desired pole location. The assumption is made that larger gains generally correspond to a demand for greater control deflection or deflection rate and this, in turn, reflects a demand for greater control power. For this metric smaller values are more desirable since small gains reflect reduced control power demands.

A third design objective area of interest is agility. Agility in this study is restricted to airframe agility; the agility metrics, unlike many in the literature, do not reflect pilot compensation effects. This was done intentionally to allow separation of flying qualities and agility metrics. Some controversy exists on the exact definition of agility and which parameters best describe it. Even without the precise definition, many agree that accelerations characterize an important aspect of transient agility. For this reason a roll acceleration metric was the agility metric used for the HARV design.

A variety of metrics can be used to indicate the regions in $\zeta-\omega$ space with the greatest tolerance to model error. For the HARV design, structured uncertainties, in the form of diagonal multiplicative error models at the input and output, were used. Structured uncertainties take advantage of user knowledge of the uncertainties and provide a less conservative measure for robustness.

Design and Evaluation Flight Conditions

The Pseudo Controls design was based on the available aerodynamic and thrust vectoring control coefficient data. This design was based on the nominal HARV weights and moments of inertia for altitudes between 10 000 and 50 000 feet, angles of attack between −10 and 90 degrees, and airspeeds between 0.2 and 0.8 Mach.

The CRAFT feedback gain design conditions were chosen based on the HARV flight test envelope which was limited to altitudes from 15 000 to 35 000 feet and Mach number less than 0.7. The feedback gains were designed at twelve design flight conditions ranging from 5 to 60 degrees angle of attack (every 5 degrees), all at 1g and 25 000 feet (See Table 4). These design points were found to be sufficient for the flight test envelope. Linear models at these design flight conditions are given in the Appendix. The nominal design weight (35 765 pounds) represents the HARV with 60% fuel load. A plot of the trim values of angle of attack versus dynamic pressure for these design conditions is given in Figure 8. Open-loop eigenvalues for these flight conditions are given in Table 5. An additional 110 flight conditions were used for control law evaluation via linear analyses. These conditions ranged from 2.5 to 65 degrees angle of attack, 15 000 to 40 000 feet altitude, 1g to 4g loading, and three weights. These evaluation conditions are listed in Table 6.

Design Eigenvalues and Eigenvectors

At low angle of attack there are three classical rigid-body lateral-directional eigenvalues: a lightly damped oscillatory pole referred to as the dutch roll pole (λ_{dr}), a first order pole with a long time constant referred to as the spiral pole (λ_{spri}), and a first order pole with a relatively short time constant referred to as the roll pole (λ_{roll}). Although with increasing angle of attack the system's eigenvalues tend to lose their classical characteristics, these terms will still be used to refer to the eigenvalues at high angle of attack that originated as classical modes at low angle of attack.

Values for desired closed-loop roll eigenvalue at the design flight conditions were chosen using the CRAFT method. Since high angle-of-attack specifications do not exist for the spiral and dutch roll modes, it was assumed that these modes should satisfy the low angle-of-attack Mil-Std 1797A specification for Level One dynamics throughout the alpha range. At each design angle of attack, the dutch roll eigenvalue was chosen to have a damping ratio of 0.7, while maintaining the open-loop natural frequency. The desired spiral eigenvalue was chosen to be stable and close to the origin. Desired closed-loop eigenvalues are listed in Table 7.

The desired roll and dutch roll eigenvectors were chosen to decouple the roll and dutch roll modes in the roll rate and sideslip responses. The desired spiral eigenvector was chosen to eliminate spiral mode contributions to sideslip. The approach used to specify eigenvectors was to set each element of the eigenvector to be 0 or 1 as appropriate to achieve the desired decoupling of the aircraft rigid-body modes. Initial choices for eigenvectors were chosen as shown in Table 8. In this table, the "x" indicates elements not weighted in the cost function and therefore are free to be determined by the eigenspace assignment algorithm. At each design condition, the phi-to-beta ratio in the dutch roll eigenvector was chosen to minimize gain magnitudes. A detailed description of the optimization approach used is given in Murphy and Davidson 1998.

Design Process

An iterative design process was used to obtain the final control law reflecting the difficult nature of flight control design for piloted nonlinear systems. Linear designs were completed by using CRAFT in combination with a linear form of Pseudo Controls. In the design process for HARV, due to the frequency separation between the rigid-body and higher-order modes, the feedback design was performed on 4th-order rigid-body lateral-directional models without actuator models, sensor models, or any higher order elements such as aero-elastic models and corresponding structural filters. This allowed extensive computations over the flight envelope and over the CRAFT design space to be performed rapidly. Gain and phase margins were analyzed with a 26th-order linear system model of the plant and control law. The 26th-order model included 4 rigid-body states, 6 actuator states, 10 measurement structural filter states, and 6 command filter states. After linear analyses were completed, a full nonlinear simulation analysis of the HARV was performed. Nonlinear simulation allowed designers to uncover any limitations inherent in the linear analysis and allowed tuning of critical elements such as pilot command gains. This portion of the development was followed by extensive piloted simulation where pilot-in-the-loop requirements were satisfied. Before going to flight with the control law a series of hardware-in-the-loop tests were performed to further increase the likelihood of success in flight. At each stage of design, revisiting a previous step was performed as required.

The control law was designed in the continuous domain. Continuous domain dynamics were discretized using a Tustin transformation at 80 Hz. This control law was primarily implemented using Matrix-X SYSTEMBUILD[†] . Code was generated for nonlinear and piloted simulation by using the FORTRAN Autocode Generator. The control law was translated into Ada for implementation on the HARV. A complete description of the control law specification is given in HARV Control Law Design Team 1996.

[†] Integrated Systems Inc.

CONTROL LAW DESCRIPTION

Figure 9 shows a functional overview of the lateral-directional control law. The control law can be thought of as consisting of three main elements : a pilot command path, a feedback path, and a feedforward path (Pseudo Controls blending). The control law accepts pilot commands for stability-axis roll rate through lateral stick deflections and for sideslip angle commands through pedal deflections. Pilot inputs are limited and shaped before being multiplied by input gains and summed with feedback signals which have been passed through structural filters and multiplied by feedback gains. The feedback measurements are body-axis roll rate, body-axis yaw rate, lateral acceleration, and estimated sideslip rate. The sum of pilot inputs and feedback commands produce stability-axis roll and yaw acceleration commands. These lateral and directional commands are distributed by the feedforward (Pseudo Controls) portion of the control law into the optimum blend of control deflections. The controls being used are aileron, rudder, differential stabilator, and yaw thrust-vectoring. The control law does not use differential leading-edge and trailing-edge flaps. Roll thrust-vectoring is not used, but a capability exists to use this control if desired.

Within the feedforward portion of the control law, measured body-axis angular rates and nominal inertial values are used to provide inertial coupling compensation. Thrust-vectoring is engaged based on its control moment producing capabilities relative to that of the aerodynamic controls. As the available aerodynamic moment decreases the thrust-vectoring increases to "fully on" at the point that the available aerodynamic moment is equal to the available thrust-vectoring moment. When the available aerodynamic moment is twice the available thrust-vectoring moment, the thrust-vectoring is turned off. To reduce potential problems due to thrust-vectoring vane heating, whenever sufficient aerodynamic control moment is available to replace yaw thrust-vectoring control, the yaw thrust-vectoring is faded out.

The three main elements of the control law (pilot command path, feedback path, and feedforward path) are discussed in more detail in the following sections.

Pilot Command Path

The function of the pilot command path is to map pilot input commands into pilot lateral and directional commands. A block diagram representation of the pilot command path is given in Figure 10a.

The lateral stick input (-3 to +3 inches) is first passed through a deadband and shaping function chosen to provide appropriate stick characteristics to the pilot. The deadband is set to ±0.025 inches. The parabolic shape function, given in Table 9, normalizes the stick input. The output is bounded to ±1.0.

The stick command limit is composed of two limiters - a rate limit and a dynamic limiter. The stick rate limit is provided to compensate for the lack of turn coordination occurring due to different actuation rates available on the ailerons and rudders. The rate limit is 12 inches/second (0 to maximum lateral stick in 0.25 seconds). The stick dynamic limiter is designed to reduce sideslip excursions that can occur during aggressive recoveries from maximum performance rolls where a large stick deflection is used. Functionally, this element allows stick deflections up to 70 percent of full throw to be passed directly, with larger deflections having the signal passed through a first-order lag. Roll Trim is added to the signal after the stick dynamic limiter.

The roll override function is designed to compensate against inertial pitch-out during rapid rolls. Commanded symmetric stabilator deflection is monitored and compared against a threshold which is a function of angle of attack. When the symmetric stabilator exceeds a preset threshold, the lateral stick command is reduced.

Yaw rates beyond that required for coordinated rolling, may be produced with yaw thrust-vectoring. To prevent excessive rates a yaw rate limiter is incorporated into the stick command path. This element monitors body-axis yaw rate (sensed yaw rate) and begins reducing lateral stick commands when yaw rate exceeds 35 degrees/second. This reduction is increased to a maximum when yaw rate reaches 60 degrees/second. The yaw rate limiting is not applied when angle of attack is negative.

Lateral stick command gains adjust the pilot commands for changes in control power with flight condition. A block diagram of this element of the pilot command path is given in Figure 10b. The lateral stick-to-lateral command gain is a function of available body roll and yaw control moments. The command gain (pds_max) is calculated in the Pseudo Controls portion of the control law. Two functions (AFUNC and GFUNC) adjust the command gain for changes in angle of attack and load factor. The angle-of-attack adjustment gains (AFUNC) were designed at the twelve linear design flight conditions (every 5 degrees from 5 to 60 degrees angle of attack). These values were chosen based upon desired roll rate and sideslip guidelines. Values between design points are determined by linear interpolation. The load factor adjustment gains (GFUNC) prevent excessive roll rates at elevated load factors. This adjustment begins at load factor of $1.5g$ and reaches a maximum command reduction of 35 percent at a load factor of $3.5g$. These values were chosen based upon piloted simulation.

The lateral stick-to-directional command cross gains were determined to minimize steady-state sideslip due to lateral stick commands. These gains are functions of angle of attack and were designed at the twelve linear design flight conditions. Values between design points are determined by linear interpolation.

The pedal input (-100 to +100 pounds) is first passed through a deadband and shaping function chosen to provide desirable pedal characteristics to the pilot. The deadband is set to ±1.0 pounds. The parabolic shape function, the same as that in the standard F/A-18, is given in Table 9. The Yaw Trim signal is added after the pedal shaping function. After addition of the yaw trim, the signal is limited to ±1.0. The pedal-to-directional command gains and pedal-to-lateral command cross gains are functions of angle of attack. These gains were designed at the twelve linear design flight conditions. Values between design points are determined by linear interpolation.

Feedback Path

A block diagram representation of the feedback path is given in Figure 11. Sensed body-axis roll and yaw rates are first passed through second-order structural notch filters (Table 10). After filtering, these rates are transformed to stability-axis rates. Gravity compensation terms are calculated and added to stability-axis yaw rate. The sensed lateral acceleration is passed through two notch filters to attenuate structural modes. A correction term is added to the filtered acceleration signal to compensate for the sensor being located off-axis. Sideslip rate is passed through a second-order structural notch filter.

The filtered feedback signals are multiplied by feedback gains and summed to yield feedback commands. The lateral and directional feedback gains are functions of angle of attack. Values between design points are determined by linear interpolation. Feedback gain values are given in Table 11.

The lateral and directional feedback commands are passed through second-order structural filters (Table 12) and first-order roll-off filters (25 radians/second). After filtering, the lateral feedback command is summed with the lateral pilot command to yield the lateral acceleration command. The directional feedback command is summed with the directional pilot command to yield the directional acceleration command.

Feedforward Path

The feedforward path (the Pseudo Controls portion of the control law) translates the lateral and directional acceleration commands into an optimum combination of control surface and yaw thrust-vectoring deflections to provide stability-axis roll and yaw accelerations. The control blending and distribution is a function of flight condition.

A block diagram representation of the feedforward path is given in Figure 12. The feedforward path can be divided into two main parts: an Interconnect and a Distributor Functional block diagrams of these are shown in Figures 13 and 14, respectively. The Interconnect converts the stability-axis roll and yaw angular acceleration commands into body-axis roll and yaw angular acceleration commands, provides compensation

for inertial coupling, provides compensation for the roll moment produced by yaw thrust-vectoring due to the engine nozzle displacement in the z-direction, and outputs roll and yaw commands in the form of pseudo control variables. These pseudo control variables (Vroll and Vyaw) are the commanded, normalized body-axis roll and yaw moments. These variables are a fraction of the available roll and yaw moments. The available moments are calculated in the Interconnect as functions of angle of attack, airspeed, altitude, Mach number, and symmetric stabilator deflection. The Interconnect also provides logic to engage the thrust-vectoring controls as a function of engine power and flight condition. The yaw thrust-vectoring can be disabled by an external input signal.

The Distributor apportions the roll and yaw pseudo control commands to the aerodynamic surfaces (aileron, rudder, and differential stabilator) and to the thrust-vectoring system (Mixer/Predictor) according to the effectiveness of the controls scheduled as functions of angle of attack and symmetric stabilator deflection and according to the yaw thrust-vectoring engage signal from the Interconnect. To prevent over-heating of the thrust-vectoring vanes, the Distributor provides "vane relief" logic to transfer slowly-varying and steady-state thrust-vectoring commands to the aerodynamic control surfaces. Thrust-vectoring is always used for transient maneuvers when permitted by the yaw thrust-vectoring engagement logic, and thrust-vectoring is used in steady-state when the aerodynamic surfaces cannot supply the required moments.

The aerodynamic surface deflection commands generated by the feedforward path are position limited. The aileron is limited to ±25.0 degrees. The rudder is limited to ±30.0 degrees. The differential stabilator is limited to ±10.0 degrees. The yaw thrust-vectoring signal to the Mixer/Predictor is not limited.

LINEAR ANALYSIS OF CONTROL LAW

Closed-loop Eigenvalues and Eigenvectors

Closed-loop eigenvalues for the twelve design flight conditions are given in Table 7. The closed-loop roll, spiral, and dutch roll eigenvalues have been placed at the desired locations for all design conditions.

The desired roll and dutch roll eigenvectors were chosen to decouple the roll and dutch roll modes in the roll rate and sideslip responses. One method of measuring the amount of decoupling achieved is to assess the cancellation of the dutch roll pole in the roll rate-to-lateral stick transfer function. The equivalent low order roll rate-to-lateral stick transfer function is given by

$$\frac{P}{\delta_{lat}} = \frac{L_\delta \, s\left(s^2 + 2\zeta_\phi \omega_\phi + \omega_\phi{}^2\right) e^{-\tau s}}{\left(s + \lambda_{sprl}\right)\left(s + \lambda_{roll}\right)\left(s^2 + 2\zeta_{dr}\omega_{dr} + \omega_{dr}{}^2\right)}$$

where $\lambda_{dr} = \zeta_{dr}\sigma_{dr} + j\omega_{dr}\sqrt{1-\zeta_{dr}^2}$.

When the dutch roll pole is canceled ($\omega_{dr} = \omega_\phi$, $\zeta_{dr} = \zeta_\phi$), the roll response is not contaminated by the dutch roll mode. A measure of cancellation is therefore given by the ratios (ω_ϕ / ω_{dr}) and ($\zeta_\phi \, \omega_\phi$) / ($\zeta_{dr} \, \omega_{dr}$). The closer the ratios are to unity, the better the dutch roll pole cancellation.

The values of these ratios for the closed-loop system, at each design condition are given in Table 13. As can be seen, there is an almost complete cancellation of the dutch roll pole in the roll rate response at most of the design flight conditions.

Stability Margins

Single-loop stability analysis was done at both the aircraft inputs and outputs. The gain and phase

margins were obtained by breaking an individual loop while leaving the remaining loops closed. The input analysis was done by breaking the individual physical control input commands to the actuators (aileron, rudder, differential stabilator, yaw thrust-vectoring) (See Figure 15). The output analysis was done by breaking the physical measurements used for feedback (body-axis roll rate, body-axis yaw rate, lateral acceleration, and estimated sideslip rate). Gain and phase margins for 5 to 60 degrees angle of attack for 15 000, 25 000, and 35 000 feet altitude at $1g$ are given in Figure 16. Gain and phase margins for 5 to 60 degrees angle of attack for 25 000 feet altitude at $1g$, $2g$, and $4g$ loading are given in Figure 17. As these figures show, the gain and phase margins are much better than the design guidelines of ± 6 dB and ± 45 degrees, respectively. These margins exclude the very low frequency range of the spiral mode. The gain and phase margins for the evaluation conditions (Table 6) were also within the guidelines for all cases.

Robustness Analysis

A real structured singular value analysis was used to assess the sensitivity of closed-loop stability to simultaneous variations of selected aircraft stability and control derivatives (Figure 18). The uncertainty model Δ associated with each derivative is the standard multiplicative one, where the inverse real structured singular value, $(\mu_R)^{-1}$, evaluated at some complex frequency is indicative of the smallest percentage derivative change required to move a pole of the closed-loop system to that complex frequency. The stability analysis generally arises from evaluating the inverse of the real structured singular value along the $j\omega$-axis in the complex plane. The minimum value along this path is the upper bound on the allowable percentage derivative change such that the system remains stable.

The general stability robustness test assumes that the nominal closed-loop system is stable. One caveat of the present stability robustness analysis, however, was the fact that the nominal closed-loop system was technically unstable due to a low frequency right-half plane spiral pole at some flight conditions. To accommodate this pole, the path along the $j\omega$-axis was initially indented into the right-half plane about the unstable pole position (Figure 19). The analysis determined the allowable percentage derivative change such that the closed-loop spiral pole did not make an excessive (greater than s=0.2 radians/second) further migration into the right-half plane and the other closed-loop poles remained stable. Due to the short duration of high alpha maneuvering, however, lack of robustness at low frequencies was later not considered important. The analysis considered only closed-loop pole excursions into the right-half plane for frequencies beyond 0.5 radians/second, which includes d itch roll frequencies.

The stability robustness analysis was performed at eight angles of attack (5, 10, 20, 35, 40, 45, 50, and 60 degrees), at three altitudes (15 000, 25 000, and 35 000 feet) at $1g$, and at 25 000 feet for $2g$ and $4g$. To consolidate the results, the lowest values of $(\mu_R)^{-1}$ from the ensemble of flight conditions corresponding to each altitude/normal acceleration pair (i.e. worst case across 5 to 60 degrees angle of attack) were plotted verses frequency. To identify key flight conditions, the angle of attack corresponding to minimum values are denoted on the plot. Figure 20 depicts the stability robustness with respect to four uncertain stability derivatives (Y_V, N_V, L_p, and N_r) and Figure 21 depicts the stability robustness with respect to four uncertain control derivatives (L_{ail}, N_{rud}, $L_{\delta stab}$, and N_{yjet}). The minimum margin across all flight conditions and parameter variations considered (the minimum inverse real structured singular value) occurred for uncertain control derivatives at 40 degrees angle of attack at 25 000 feet and a loading of $4g$. The value for this case is 0.83 at a frequency of 2.95 radians/second. This indicates the system will remain stable in the face of up to 83% simultaneous change in the four control derivatives. This result is considered quite good. Tables 14 and 15 summarize the margins and critical frequencies for all flight conditions considered.

Servo-Elastic Analysis

A servo-elastic analysis was conducted to assess the effect of structural modes on closed-loop stability. For this analysis, a 50th-order servo-elastic model was placed in parallel with the series combination of

rigid-body plant and actuator dynamics. Margins were obtained by breaking an individual loop while leaving the remaining loops closed. The input analysis was done by breaking the individual input commands (commanded stability-axis roll and yaw accelerations). The output analysis was done by breaking the physical measurements used for feedback (body-axis roll rate, body-axis yaw rate, lateral acceleration, and sideslip rate) (See Figure 22).

This analysis revealed that the system failed to meet the -10 dB structural margin requirement. Worst case was found to be at 40 degrees angle of attack. Structural filters were designed to notch-out high frequency structural modes and achieve the required structural margin at this flight condition (Tables 10 and 12). The analysis was then repeated with the structural filters. The output servo-elastic frequency responses with and without filters for 5, 20, 40, and 60 degrees angle of attack are given in Figures 23-26. The input servo-elastic frequency responses with and without filters for 5, 20, 40, and 60 degrees angle of attack are given in Figures 27 and 28.

NONLINEAR BATCH SIMULATION RESULTS

Evaluations were conducted by using the nonlinear batch simulation described earlier to assess roll performance, bank angle overshoot, and angle-of-attack and sideslip excursions. These evaluations were conducted using the longitudinal control law described in Ostroff et al. 1994.

Step Input Time Responses

System time responses for a full lateral stick deflection to command maximum roll rate are given in Figures 29-31 for 5, 35, and 60 degrees angle of attack to illustrate system performance. The input is maximum lateral stick, input at one second and removed at 9 seconds. The time responses plotted are lateral stick input, stability-axis roll rate (degrees/second), and sideslip angle (degrees). Time responses are shown for altitudes of 15 000, 25 000, and 35 000 feet. The following summarizes performance results for 25 000 feet. At 5 degrees angle of attack the maximum stability-axis roll rate at ϕ_W of 90 degrees is approximately 165 degrees/second. The time to roll through 90 degrees ϕ_W is 0.99 seconds. At 35 degrees angle of attack the maximum stability-axis roll rate at ϕ_W of 90 degrees is approximately 45 degrees/second. The time to roll through 90 degrees ϕ_W is 3.25 seconds. At 60 degrees angle of attack the maximum stability-axis roll rate at $\phi_W = 90$ degrees is approximately 35 degrees/second. The time to roll through 90 degrees ϕ_W is 4.6 seconds.

Comparison with Nonlinear Design Guidelines

Nonlinear guidelines, used as performance metrics for large amplitude maneuvers, were developed using previous experience from simulations at NASA Langley combined with knowledge of HARV characteristics (Hoffler et al. 1994). These guidelines are therefore a blend of HARV control law design goals and what are currently considered (by the authors) good preliminary roll and pitch agility requirements for an aircraft capable of post-stall maneuvering. In the following discussion some of the nonlinear guidelines are summarized, and some direction on making trade-offs between them is given. HARV and F/A-18 (A Model) simulation performance are also shown relative to selected guidelines.

Nonlinear guidelines used for the roll axis included maximum wind-axis roll rate ($p_{W\text{-}max}$) during a roll through $\Delta\phi_W = 90°$, time to bank through $\Delta\phi_W = 90°$ ($t_{\Delta\phi_W = 90°}$), wind-axis bank angle overshoot ϕ_{OS}, and maximum α and β excursions. Values for these guidelines for $1g$ trim throughout the α range were defined as well as values for Mach 0.6 from low α to $\alpha = 35$ degrees.

The lateral-directional coupling guidelines for full-lateral stick with longitudinal stick fixed are shown in Table 16. These guidelines were met with the control law throughout the flight envelope.

The $t_{\Delta\phi_W} = 90°$ and $p_{W\text{-}max}$ guidelines and performance achieved for the F/A-18 and the HARV are shown in Figures 32 and 33. The HARV met both of these guidelines through 35° α, and the $p_{W\text{-}max}$ guideline was nearly met throughout the angle-of-attack range. The F/A-18 failed to meet both guidelines above approximately 15° α.. It falls short of the guideline due to insufficient directional control power required to coordinate rolls above $\alpha \approx 10°$. The HARV $t_{\Delta\phi_W} = 90°$ performance fell outside the guideline above 35° α primarily due to lack of available control power. However, time to bank could be improved for $\alpha > 20°$ if all available performance was used without regard to another guideline addressing controllability and predictability.

Wind-axis bank angle overshoot is a guideline developed during the HARV control law design effort that directly addresses lateral-directional predictability at moderate to high angles of attack. Wind-axis bank angle overshoot is defined here as the amount of wind-axis bank angle used to stop a maximum performance roll with a full stick reversal applied when passing through 90 degrees wind-axis bank angle change. If the overshoot is excessive, pilots will have difficulty judging the lead required to capture the desired bank or heading angle. The result would be poor predictability and a tendency to overshoot or undershoot the target bank angle.

Figure 34 shows the wind-axis bank angle overshoot criteria and the achieved values. Because the available control power is fixed there is a direct trade-off between bank angle overshoot and maximum roll rate. The bank angle overshoot as defined herein equates to pilot lead requirement necessary to make a capture within desired tolerances. Maximum lead of around 40 to 45 degrees was considered acceptable by the pilots in this design effort. Although the pilots could learn to consistently predict different lead requirements ($\leq 45°$) at each α, in air combat maneuvering (ACM), angle-of-attack may not always be known by the pilot and constantly changes. Therefore, it was considered important to have fairly consistent overshoots throughout the moderate to high angle-of-attack range making predictability consistent anytime lateral stick inputs produced significant amounts of yaw rate. High body yaw rates as opposed to body roll rates serve as a visual cue to the pilot that angle of attack is high without having to refer to the α display. As can be seen from Figure 34, the HARV meets the guideline with fairly consistent overshoots throughout the moderate to high angle-of-attack range.

Complete descriptions of the high alpha nonlinear design guidelines can be found in Foster 1991.

NONLINEAR PILOTED SIMULATION RESULTS

Pilot-in-the-loop evaluations were conducted using NASA Langley's Differential Maneuvering Simulator and the nonlinear HARV model described earlier. The evaluations used a series of piloted tasks designed to test the longitudinal and lateral-directional control systems throughout the HARV flight envelope. The tasks were designed for this effort with the intent of having broad applicability because no concise set of maneuvers previously existed to evaluate configurations in the moderate to high angle-of-attack regions. The lateral-directional piloted evaluation maneuvers included heading captures, large amplitude rolls with bank angle captures, and target gross acquisition and tracking tasks.

The piloted maneuver set was developed with goals of allowing evaluation of each axis of the control law individually where possible, using consistent maneuvers and task guidelines across the flight envelope when possible, and obtaining piloted evaluations in a short time. A brief discussion of the maneuvers and associated Cooper-Harper task tolerances (Cooper and Harper 1969) include piloting technique, associated task criteria, and pros and cons of the maneuvers. The task tolerances were intentionally restrictive to make pilot gains high, thus aggravating any Pilot Induced Oscillation (PIO) tendencies that might exist. The very tight criterion also tends to produce less favorable pilot subjective ratings (Cooper-Harper rating's). The maneuvers were conducted at altitudes from 15 000 to 40 000 feet, but only results from 25 000 feet are presented. Cooper-Harper ratings from simulation are shown for the control law design flown on the HARV in the Spring of 1994. Preliminary flight test results are described in Murphy et al. 1994.

Five NASA test pilots were involved in this study. Two have extensive air combat training and experience, and all have high performance aircraft experience. One pilot has many years of experience with

simulated high-α airplanes, and one has extensive experience in simulated as well as actual high-α capable airplanes. Two of the other pilots have at least three years of experience with simulated high-α airplanes. These evaluations were the first experience performing some of these tasks with an airplane capable of agile and precise maneuvering at high-α for one pilot. Four of the five pilots have experience with the use of simulated within-visual-range air-combat scenarios of high-α airplanes against one or two conventional airplanes.

The evaluations were conducted as follows: Initially the task was flown repeatedly for familiarity with the required piloting techniques, flight condition, and configuration. Once the pilots felt they were proficient, the task was repeated a few times to rate it. After the evaluations were completed with all pilots, limited one-versus-one simulated engagements were flown against a basic F/A-18. The control law was extensively exercised during the one-versus-one engagements and found to be very departure resistant. The one-versus-one results are not presented herein, but control system related pilot comments and observations from the one-versus-one are discussed in Hoffler et al. 1994.

Results from piloted simulation maneuvers are presented in terms of Cooper-Harper Ratings (CHR) and pilot comments. The CHR scale is a numerical scale from one to ten with one being the best rating and 10 the worst (Figure 35). In practice CHR's from 1 through 3 are referred to as "Level One", ratings from 4 through 6 are labeled "Level Two", and ratings from 7 to 9 are considered "Level Three". CHR's less than or equal to 4 indicate desired performance was achieved. For space considerations, only bar charts showing the average rating from the five pilots involved are shown. All ratings are shown in tabular form in Table 17.

The Cooper-Harper rating variation between pilots is shown in Table 18. For all five pilots the span between the maximum and minimum rating was less than or equal to three (±1.5 from mean value) 92% of the time. On four of the maneuvers the pilot with no prior experience flying high-α airplanes gave ratings significantly different from the other four. Neglecting those four ratings, differences greater than 3 were not seen and 84% of the maneuvers yielded differences less than or equal to 2 (±1 from the mean value). Overall the rating spread was small implying the tasks are well defined (Cooper and Harper 1969).

Seven single airplane maneuvers (maneuvers where no target was involved) were developed. Early in the design process these maneuvers were used almost exclusively because they could be done very quickly and there was only one dynamic system (the airplane) affecting the result. This made assessment and correction of any problems more straight-forward than if a target airplane were involved. The tasks fell into two categories: 1) Maneuvers that primarily isolated the longitudinal axis; and 2) Maneuvers that concentrated on the lateral-directional axis but addressed inertial and kinematic coupling. Only the lateral-directional axis maneuvers are discussed in this report.

Single Aircraft Lateral-Directional Evaluation Maneuvers

The lateral-directional evaluation maneuvers consisted of rolls to capture target bank angles at various flight conditions. Angle-of-attack control was required during the rolls because α changes during the rolls can significantly alter aircraft roll performance and energy state as well as lead to departures. Also during gross acquisition tasks (pointing) at moderate and high angle of attack, both the lateral-directional and longitudinal axes directly affect the capture due to the coning motion (Figure 36). Therefore during the roll tasks the pilots were required to give CHR's on two sub-tasks, α regulation and the wings-level ϕ capture. The pilots were required to maintain the target α within ±2° for desired and ±6° for adequate performance during all roll tasks. They were also required to capture the desired ϕ within ±10° for desired and ± 20° for adequate performance, with no overshoots or undershoots. These task tolerances were intentionally tight to keep the pilot's gain high.

1g 360° Roll Tasks

A complete 360° roll was used because it gave the pilots a convenient bank angle to capture, wings level with the horizon, thus simplifying the task both from a piloting and data analysis point of view. It is recognized that this is an extreme maneuver, beyond what would normally be done in air combat

maneuvering (ACM) (rolls beyond 180° are not expected in ACM). The 1g 360° roll maneuvers started from 1g trim at the desired α. If not already at maximum thrust, maximum thrust was applied, time was allowed for the engine to reach maximum thrust, then maximum lateral stick was applied.

This task exposed roll coordination and predictability problems and lateral-directional PIO sensitivities in the control system. Average CHR's for the 1g rolls from the simulation are shown in Figure 37. The majority of the ratings were in the Level One region with a few results edging into the Level Two handling qualities region. The roll rating at $\alpha = 5°$ was Level Two primarily because of the task itself. Maximum stick rolls here produce very high roll rates making ϕ captures difficult. The high rates made predictability difficult, and given the simulation transport delay the results at this α may be unreliable. With less than maximum lateral stick input the maneuver could be done within the desired parameters by all pilots. The pilots pointed out that maximum roll rate at low angles of attack would only be used defensively, that is, for offensive maneuvers maximum roll rate would not likely be achieved at this flight condition. At 15° α, desired criterion was met by most pilots in both axes. But, ϕ capture difficulty was still seen due to high roll rates. Average ratings were Level One, and desired criterion was met by all pilots from 25° through 65° α with the exception of the roll rating at 65°. Here the yaw vectoring control power is limited, and predictability became a problem.

Loaded Roll Tasks

Loaded rolls were conducted at Mach 0.4 and 0.6 and various angles of attack. These maneuvers started with the airplane trimmed at 1g and typically faster than the desired Mach. The pilot rolled to a ϕ of around 60° (varied with target α) and pulled to the desired α, then waited to decelerate to the desired Mach number. At the desired Mach, maximum lateral stick input was applied to roll back through wings level and capture $\phi = 90°$. This gave a $\Delta\phi$ of approximately 150° for the task. The Cooper-Harper criteria for the two sub-tasks was the same as the 1g 360° rolls.

Average ratings from the five pilots are shown in Figure 38. The ratings are similar to the 1g roll ratings and generally on the Level One/Level Two boundary. These tasks were significantly more difficult to carry out than the 1g roll tasks because of the set up required to get to the initial condition. The desired α had to be captured quickly due to the high Mach bleed rate seen at the higher α's required for these loaded evaluations.

Target Tracking and Acquisition Tasks

With the single airplane maneuvers completed, simulated target acquisition and tracking tasks were conducted.

Moderate Angle-of-Attack / Elevated-g Tracking Tasks

These tasks were developed to look at tracking in the 15° to 25° angle-of-attack range. Two tasks were used, both tracking a target maneuvering at 3g, one with a Mach range from 0.55 to 0.65 (Mach 0.6 task) and one from Mach 0.4 to 0.5 (Mach 0.45 task). Initial range to the target was 600 feet and a maximum range of 1800 feet was allowed during the task. During these tasks the target rolled into a left 3g turn and held it for 30 seconds; at 30, 40, and 50 seconds elapsed time the turn direction was reversed with a smooth moderate rate reversal. The total task time was 70 seconds. The pilots gave both a longitudinal and lateral-directional rating for each maneuver.

The Cooper-Harper task tolerances used for this task were to keep the target within a 12.5 milliradian reticle (±0.36° of aim point) 50% of the time for desired and 10% of the time for adequate performance. The reticle was depressed 35 milliradians. Tracking time during the reversals was not counted. This is a precision tracking task.

Average CHR's from the five pilots showed desired performance was generally achievable in the roll axis (all but one pilot) (Figure 39). The pilots considered the control law to have good tracking characteristics. The only significant lateral-directional problem with this version of the control law is some "wandering" in the roll axis.

High Angle-of-Attack Tracking and Acquisition Tasks

These tasks were developed by McDonnell Douglas Aerospace under contract to NASA Langley and were used during this control law development. Longitudinal and lateral tasks have been developed at 30, 45, and 60 degrees angle-of-attack; however, only the 30 and 45 degree angle-of-attack tasks were available at the time of this evaluation. A general description of the maneuvers follows. Detailed task descriptions can be found in Wilson et al. 1993a and 1993b. The tasks were used to evaluate longitudinal and lateral-directional target acquisition and tracking characteristics. For all tasks the target started in front of the HARV and rolled into a nose low descending right turn at a specified α, airspeed, and power setting. This was done to put the target in the proper position for the HARV to acquire or track at the desired α. Pre-recorded target time histories were used for the target aircraft and therefore were perfectly repeatable.

Tracking: For the tracking tasks the HARV selected maximum afterburner (A/B) and rolled in behind the target. The HARV delayed a pitch toward the target so that pulling to the target would result in a HARV angle of attack near the desired α to begin tracking. When the α required to track the target was more than 5° from the desired α , the task was terminated. Desired α's of 30 and 45 degrees were used. Desired criteria for these tasks required keeping the pipper within ±5 milliradians of the aim point 50% of the time and within ±25 milliradians of the aim point the rest of the time with no objectionable PIO. Adequate criteria required keeping the pipper within ±5 milliradians of the target 10% of the time and within ±25 milliradians the remainder of the task. For both tasks concentric 12.5 and 50 milliradian diameter reticles depressed 80 milliradians were provided to the pilot.

Average lateral-directional ratings from the five pilots are shown in Figure 40 for both α's. The lateral-directional ratings were mostly Level Two. Desired criteria were met by all but pilot five; his ratings were not far from the others. A difficulty in tracking at these conditions is that lateral-directional and longitudinal motions couple in a way foreign to pilots with no high-α experience. At these (extreme by current airplane capabilities) α's, a roll input significantly affects the longitudinal tracking due to the nose moving around the "cone" (Figure 36).

Acquisition: For the high-α acquisition tasks the targets flew paths similar to those used in the tracking tasks. The lateral-directional acquisition tasks required the HARV to pull to the desired α and then to roll at that α to capture the target. These tasks were similarly dependent on target turn rate and HARV motion and for the 45° α tasks, the target was out of view below the nose during part of the task. These tasks required precise timing in order to make the acquisitions at the desired α. With practice the pilots could do the tasks consistently, and the tasks worked well.

The Cooper-Harper desired performance criteria for the 30° α acquisition tasks required aggressively acquiring the aim point within ±25 milliradians laterally of the reticle with no overshoot and in a desirable time to accomplish the task. Adequate performance criteria allowed one overshoot/undershoot. A 50 milliradian reticle depressed 35 milliradians was provided to the pilot for these tasks. The Cooper-Harper task tolerances for the 45° α acquisition tasks were similar except the criteria was within ±40 milliradians of the aim point. An 80 milliradian reticle depressed 80 milliradians was provided to the pilot for these tasks.

The average CHR's from the 5 pilots for the lateral-directional acquisitions at both α's are shown in Figure 41. Most ratings for all these tasks were Level Two. Predictability was a problem in both axes. Pilot five gave ratings that were significantly different from the other four pilots for the 45° roll acquisition tasks. For all pilots, unless timing was precise, typically one overshoot occurred followed by a good acquisition.

CONCLUDING REMARKS

This report contains a description of a lateral-directional control law designed for the NASA High-Alpha Research Vehicle (HARV). This control law was designed using two separate design tools, CRAFT and Pseudo Controls. The combined CRAFT/Pseudo Controls design technique is a hybrid technique that combines both linear and nonlinear design methods. The CRAFT (Control Power, Robustness, Agility, and Flying Qualities Tradeoffs) design process is a linear design approach based on eigenspace assignment for determining measurement feedback gains. The CRAFT design approach makes use of Direct Eigenspace Assignment, which allows direct specification of closed-loop dynamics, in combination with graphical overlays of metric surfaces which capture important design objectives. Pseudo Controls is a nonlinear control blending strategy for distributing control system commands in a near-optimal fashion to the appropriate control effectors. In this method, flight controls are ganged together to generate body-axis roll and yaw moments as independent commands.

Results of linear analyses, nonlinear batch simulation, and piloted simulation of this control law show the following:

1) The combined CRAFT/Pseudo Controls methodology has been demonstrated to be a useful technique for aircraft control law design. The control laws developed with this approach have demonstrated good performance, robustness, and flying qualities in piloted simulation.

2) The closed-loop system meets the single-loop gain and phase margin guidelines of ±6 dB and 45 degrees, respectively, at both the plant inputs and outputs.

3) Based upon a real structured singular value analysis, the closed-loop system has good robustness to changes in plant stability and control derivatives.

4) With the addition of the structural filters, the control law meets the structural mode attenuation guideline of −10 dB.

5) Nonlinear batch simulation analysis shows the control law exhibits good performance and meets most of the design guidelines over the entire range of angle of attack.

6) The control law has been extensively exercised in piloted simulation and shown to be very departure resistant. The characteristics predicted from piloted simulation generally held true during flight test. Piloted simulation results are summarized in the following by task:

Roll Tasks

1g 360 Degree Rolls: The majority of the Cooper-Harper rating's were in the Level One region with a few results edging into the Level Two handling qualities region. This task did a good job of uncovering roll coordination and predictability problems and lateral-directional Pilot Induced Oscillation (PIO) sensitivities in the control system.

Loaded Rolls: Average Cooper-Harper rating's from the five pilots are similar to the 1*g* roll ratings and generally on the Level One/Level Two handling qualities boundary. These tasks were significantly more difficult to carry out than the 1*g* roll tasks because of the set up required to get to the initial condition.

Moderate Angle-of-Attack (15-25 degrees)/ Elevated-*g* Tracking and Acquisition Tasks

Average Cooper-Harper rating's from the five pilots showed desired performance was generally achievable in the roll axis. The pilots considered the control law to have good tracking characteristics.

High Angle-of-Attack (30 and 45 degrees) Tracking and Acquisition Tasks

Tracking: Average lateral-directional Cooper-Harper rating's from the five pilots were mostly Level Two. Desired criteria were met by all but pilot five; his ratings were not far from the others. A difficulty in tracking at these conditions is that lateral-directional and longitudinal motions couple in a way foreign to pilots with no high angle-of-attack experience.

Acquisition: The average Cooper-Harper rating's from the five pilots for the lateral-directional acquisitions at both angles-of-attack were mostly Level Two. Predictability was a problem in both axes. For all pilots, unless timing was precise, typically one overshoot occurred followed by a good acquisition.

This control law was flight tested during the Summer of 1994 at NASA Dryden Flight Research Center. Flight test results are presented in Murphy et al. 1994.

NASA Langley Research Center

Hampton, VA 23681-0001

APPENDIX

This Appendix presents the twelve linear lateral/directional design models. The models are based on steady-state wings-level trim flight conditions at 25 000 feet. They include the four standard lateral-directional rigid-body degrees of freedom.

The models are given by:

$$\dot{x} = A_{ol}\, x + B_{ap}\, \delta \quad \text{(system dynamics)}$$

$$\delta = G_{fl}\, u \quad \text{(blended control inputs)}$$

$$z = M_{ol}\, x + N_{col}\, u \quad \text{(system measurements)}$$

$$u_c = Gz \quad \text{(feedback control law)}$$

$$u = u_p + u_c \quad \text{(total control input)}$$

$$u_p = \text{pilot input}$$

The system states are:

$$x = [\, v \; p_{stab} \; r_{stab} \; \phi \,]^T$$

where v = side velocity (ft/sec), p_{stab} = stability-axis roll rate (rad/sec), r_{stab} = stability-axis yaw rate (rad/sec), and ϕ = bank angle (rad).

The physical controls are:

$$\delta = \left[\delta_{ail} \quad \delta_{rud} \quad \delta_{dt} \quad \delta_{ytv}\right]^T$$

where δ_{ail} = aileron deflection (deg), δ_{rud} = rudder deflection (deg), δ_{dt} = differential stabilator deflection (deg), and δ_{ytv} = yaw thrust vectoring deflection (deg).

The system controls are:

$$u = [\, a_{roll} \; a_{yaw} \,]^T$$

where a_{roll} = stability-axis roll acceleration (rad/sec^2) and a_{yaw} = stability-axis yaw acceleration (rad/sec^2). The system, expressed as a function of system states and blended control inputs, is given by:

$$\dot{x} = A_{ol}\, x + B_{ap}\, G_{fl}\, u = A_{ol}\, x + B_{col}\, u$$

The measurements used for feedback are:

$$z = [\, p_{stab} \; r_{stab} \; a_y \; \dot{\beta} \,]^T$$

where p_{stab} = stability-axis roll rate (rad/sec), r_{stab} = stability-axis yaw rate (rad/sec), a_y = lateral acceleration (g's), and β = sideslip rate (rad/sec).

Angle of attack (ALPHA) = 5.0 (degrees)
Dynamic Pressure (QBAR) = 191.07 (psf)
Trim Velocity (VTOT) = 598.07 (ft/sec)

A_{OL} =

-0.1305	0.1512	-597.582	32.1667
-0.0187	-1.5271	0.6757	0.0000
0.0050	0.1152	-0.1529	0.0000
0.0000	1.0000	0.0000	0.0000

B_{AP} =

-0.0551	0.2975	-0.1025	0.2463	0.0024
0.2746	0.0314	0.2225	-0.0059	0.0177
-0.0283	-0.0242	-0.0161	-0.0294	-0.0019
0.0000	0.0000	0.0000	0.0000	0.0000

G_{FL} =

4.0251	2.4502
-5.6822	-62.0789
0.8580	4.8530
0.0000	0.0000
0.0000	0.0000

B_{COL} =

-2.0005	-19.1022
1.1179	-0.1941
0.0096	1.3527
0.0000	0.0000

M_{OL} =

0.0000	1.0000	0.0000	0.0000
0.0000	0.0000	1.0000	0.0000
-0.0021	0.0535	-0.0462	0.0000
-0.0002	0.0003	-0.9992	0.0538

N_{COL} =

0.0000	0.0000
0.0000	0.0000
-0.0614	-0.0669
-0.0033	-0.0319

Angle of attack (ALPHA) = 10.0 (degrees)
Dynamic Pressure (QBAR) = 94.53 (psf)
Trim Velocity (VTOT) = 420.67 (ft/sec)

A_{OL} =

-0.0955	0.1610	-420.288	32.1678
-0.0194	-0.8687	0.6852	0.0000
0.0062	0.1333	-0.1871	0.0000
0.0000	1.0000	0.0000	0.0000

B_{AP} =

-0.0286	0.1409	-0.0358	0.2499	0.0004
0.1350	0.0146	0.1010	-0.0085	0.0178
-0.0261	-0.0130	-0.0161	-0.0290	-0.0032
0.0000	0.0000	0.0000	0.0000	0.0000

G_{FL} =

6.9740	2.5229
-21.1742	-116.8032
2.2404	8.4609
0.0000	0.0000
0.0000	0.0000

B_{COL} =

-3.2622	-16.8276
0.8596	-0.5050
0.0561	1.3108
0.0000	0.0000

M_{OL} =

0.0000	1.0000	0.0000	0.0000
0.0000	0.0000	1.0000	0.0000
-0.0012	0.0295	-0.0392	0.0000
-0.0002	0.0004	-0.9991	0.0765

N_{COL} =

0.0000	0.0000
0.0000	0.0000
-0.0527	-0.0305
-0.0078	-0.0400

ALPHA = 15.0 (degrees)
Dynamic Pressure (QBAR) = 69.71 (psf)
Trim Velocity (VTOT) = 361.25 (ft/sec)

A_{OL} =

-0.0702	0.1331	-361.025	32.1679
-0.0185	-0.5227	0.6580	0.0000
0.0069	0.1218	-0.2358	0.0000
0.0000	1.0000	0.0000	0.0000

B_{AP} =

-0.0198	0.0873	-0.0149	0.2488	-0.0012
0.0817	0.0078	0.0618	-0.0105	0.0173
-0.0236	-0.0089	-0.0160	-0.0280	-0.0045
0.0000	0.0000	0.0000	0.0000	0.0000

G_{FL} =

10.2115	-0.9327
-27.6436	-103.1960
3.2085	6.6783
-3.0905	-11.0352
0.0000	0.0000

B_{COL} =

-3.4330	-11.8391
0.8502	0.3483
0.0403	1.1444
0.0000	0.0000

M_{OL} =

0.0000	1.0000	0.0000	0.0000
0.0000	0.0000	1.0000	0.0000
-0.0007	0.0169	-0.0407	0.0000
-0.0002	0.0004	-0.9994	0.0890

N_{COL} =

0.0000	0.0000
0.0000	0.0000
-0.0434	0.0220
-0.0095	-0.0328

Angle of attack (ALPHA) = 20.0 (degrees)
Dynamic Pressure (QBAR) = 59.58 (psf)
Trim Velocity (VTOT) = 333.97 (ft/sec)

A_{OL} =

-0.0559	0.0400	-334.021	32.1674
-0.0236	-0.2995	0.6025	0.0000
0.0095	0.0932	-0.2797	0.0000
0.0000	1.0000	0.0000	0.0000

B_{AP} =

-0.0076	0.0559	-0.0082	0.2393	0.0039
0.0464	0.0037	0.0454	-0.0120	0.0159
-0.0183	-0.0061	-0.0169	-0.0261	-0.0062
0.0000	0.0000	0.0000	0.0000	0.0000

G_{FL} =

15.0221	-5.6111
-33.4460	-90.6366
3.6615	2.6429
-6.9681	-18.4940
0.0000	0.0000

B_{COL} =

-3.6822	-9.4746
0.8233	-0.2519
0.0488	1.0950
0.0000	0.0000

M_{OL} =

0.0000	1.0000	0.0000	0.0000
0.0000	0.0000	1.0000	0.0000
-0.0005	0.0069	-0.0477	0.0000
-0.0002	0.0001	-1.0002	0.0963

N_{COL} =

0.0000	0.0000
0.0000	0.0000
-0.0411	0.0243
-0.0110	-0.0284

Angle of attack (ALPHA) = 25.0 (degrees)
Dynamic Pressure (QBAR) = 50.67 (psf)
Trim Velocity (VTOT) = 308.00 (ft/sec)

A_{OL} =

-0.0472	-0.0569	-308.198	32.1682
-0.0191	-0.2337	0.5856	0.0000
0.0103	0.0901	-0.3405	0.0000
0.0000	1.0000	0.0000	0.0000

B_{AP} =

0.0108	0.0375	0.0061	0.2568	0.0022
0.0315	0.0005	0.0354	-0.0158	0.0173
-0.0162	-0.0035	-0.0179	-0.0263	-0.0085
0.0000	0.0000	0.0000	0.0000	0.0000

G_{FL} =

15.3733	-15.0921
-41.2548	-84.1465
3.5039	-1.3391
-10.5999	-22.0790
0.0000	0.0000

B_{COL} =

-4.0828	-8.9986
0.7569	-0.2134
0.1112	1.1441
0.0000	0.0000

M_{OL} =

0.0000	1.0000	0.0000	0.0000
0.0000	0.0000	1.0000	0.0000
-0.0002	0.0007	-0.0544	0.0000
-0.0002	-0.0002	-1.0006	0.1044

N_{COL} =

0.0000	0.0000
0.0000	0.0000
-0.0267	0.0297
-0.0133	-0.0292

Angle of attack (ALPHA) = 30.0 (degrees)
Dynamic Pressure (QBAR) = 42.48 (psf)
Trim Velocity (VTOT) = 282.00 (ft/sec)

A_{OL} =

-0.0403	-0.1337	-282.258	32.1549
-0.0099	-0.3858	0.7811	0.0000
0.0060	0.2001	-0.5262	0.0000
0.0000	1.0000	-0.0280	0.0000

B_{AP} =

0.0195	0.0270	0.0182	0.2530	0.0013
0.0211	-0.0006	0.0287	-0.0170	0.0172
-0.0137	-0.0022	-0.0185	-0.0249	-0.0103
0.0000	0.0000	0.0000	0.0000	0.0000

G_{FL} =

15.2351	-24.5759
-47.9817	-75.1111
2.9207	-5.1282
-14.1410	-23.8682
0.0000	0.0000

B_{COL} =

-4.5212	-8.6376
0.6768	-0.2130
0.1948	1.1910
0.0000	0.0000

M_{OL} =

0.0000	1.0000	0.0000	0.0000
0.0000	0.0000	1.0000	0.0000
-0.0007	0.0041	-0.0675	0.0000
-0.0001	-0.0005	-1.0009	0.1140

N_{COL} =

0.0000	0.0000
0.0000	0.0000
-0.0145	0.0296
-0.0160	-0.0306

Angle of attack (ALPHA) = 35.0 (degrees)
Dynamic Pressure (QBAR) = 38.17 (psf)
Trim Velocity (VTOT) = 267.31 (ft/sec)

A_{OL} =

-0.0423	-0.2075	-267.564	31.9378
-0.0027	-0.3023	0.8107	0.0000
0.0019	0.1766	-0.6487	0.0000
0.0000	1.0000	-0.1202	0.0000

B_{AP} =

0.0246	0.0214	0.0250	0.2490	0.0013
0.0155	-0.0011	0.0245	-0.0187	0.0160
-0.0124	-0.0015	-0.0196	-0.0232	-0.0117
0.0000	0.0000	0.0000	0.0000	0.0000

G_{FL} =

14.9838	-35.8822
-59.0482	-69.9067
1.7375	-8.9323
-16.4497	-22.9385
0.0000	0.0000

B_{COL} =

-4.9497	-3.3163
0.6501	-0.2688
0.2488	1.2571
0.0000	0.0000

M_{OL} =

0.0000	1.0000	0.0000	0.0000
0.0000	0.0000	1.0000	0.0000
-0.0012	-0.0048	-0.0715	0.0000
-0.0002	-0.0008	-1.0010	0.1195

N_{COL} =

0.0000	0.0000
0.0000	0.0000
-0.0058	0.0298
-0.0185	-0.0311

Angle of attack (ALPHA) = 40.0 (degrees)
Dynamic Pressure (QBAR) = 36.52 (psf)
Trim Velocity (VTOT) = 261.48 (ft/sec)

A_{OL} =

-0.0435	-0.2705	-261.691	31.4209
0.0003	-0.3069	0.6522	0.0000
-0.0018	0.2127	-0.6252	0.0000
0.0000	1.0000	-0.2193	0.0000

B_{AP} =

0.0257	0.0181	0.0277	0.2457	0.0013
0.0125	-0.0018	0.0210	-0.0202	0.0148
-0.0123	-0.0008	-0.0207	-0.0214	-0.0129
0.0000	0.0000	0.0000	0.0000	0.0000

G_{FL} =

17.1216	-50.0765
-72.7024	-55.6999
0.8089	-13.0617
-18.0346	-21.0078
0.0000	0.0000

B_{COL} =

-5.2843	-7.8158
0.7229	-0.3767
0.2184	1.3802
0.0000	0.0000

M_{OL} =

0.0000	1.0000	0.0000	0.0000
0.0000	0.0000	1.0000	0.0000
-0.0018	-0.0081	-0.0628	0.0000
-0.0002	-0.0010	-1.0008	0.1202

N_{COL} =

0.0000	0.0000
0.0000	0.0000
-0.0016	0.0377
-0.0202	-0.0299

Angle of attack (ALPHA) = 45.0 (degrees)
Dynamic Pressure (QBAR) = 36.54 (psf)
Trim Velocity (VTOT) = 261.54 (ft/sec)

A_{OL} =

-0.0383	-0.2061	-261.391	30.5801
-0.0105	0.1843	0.0830	0.0000
0.0088	-0.2481	-0.1543	0.0000
0.0000	1.0000	-0.3264	0.0000

B_{AP} =

0.0079	0.0162	0.0264	0.2404	0.0013
0.0109	-0.0030	0.0247	-0.0215	0.0135
-0.0129	0.0004	-0.0269	-0.0194	-0.0140
0.0000	0.0000	0.0000	0.0000	0.0000

G_{FL} =

21.0191	-66.8294
-88.2694	-33.0892
-5.9323	-17.0833
-19.0749	-18.6501
0.0000	0.0000

B_{COL} =

-6.0103	-5.9983
0.7541	-0.6494
0.2208	1.6680
0.0000	0.0000

M_{OL} =

0.0000	1.0000	0.0000	0.0000
0.0000	0.0000	1.0000	0.0000
-0.0012	-0.0350	-0.0210	0.0000
-0.0001	-0.0008	-0.9994	0.1169

N_{COL} =

0.0000	0.0000
0.0000	0.0000
-0.0045	0.0831
-0.0230	-0.0229

Angle of attack (ALPHA) = 50.0 (degrees)
Dynamic Pressure (QBAR) = 36.59 (psf)
Trim Velocity (VTOT) = 261.71 (ft/sec)

A_{OL} =

-0.0333	0.0412	-261.3256	29.4799
-0.0077	-0.0330	0.2272	0.0000
0.0084	-0.0162	-0.3423	0.0000
0.0000	1.0000	-0.4366	0.0000

B_{AP} =

-0.0118	0.0147	0.0370	0.2348	0.0012
0.0087	-0.0035	0.0242	-0.0227	0.0121
-0.0129	0.0014	-0.0292	-0.0174	-0.0150
0.0000	0.0000	0.0000	0.0000	0.0000

G_{FL} =

19.4371	-77.3519
-102.6940	-9.2118
-10.7424	-13.7265
-20.3969	-16.7274
0.0000	0.0000

B_{COL} =

-6.9250	-3.6611
0.7313	-0.5911
0.2730	1.6771
0.0000	0.0000

M_{OL} =

0.0000	1.0000	0.0000	0.0000
0.0000	0.0000	1.0000	0.0000
-0.0008	-0.0122	-0.0208	0.0000
-0.0001	0.0002	-0.9985	0.1126

N_{COL} =

0.0000	0.0000
0.0000	0.0000
-0.0156	0.1270
-0.0265	-0.0140

Angle of attack (ALPHA) = 55.0 (degrees)
Dynamic Pressure (QBAR) = 37.70 (psf)
Trim Velocity (VTOT) = 265.67 (ft/sec)

A_{OL} =

-0.0381	0.1644	-265.408	28.4186
-0.0065	-0.0508	0.2138	0.0000
0.0087	0.0197	-0.3784	0.0000
0.0000	1.0000	-0.5303	0.0000

B_{AP} =

-0.0145	0.0143	0.0725	0.2314	0.0012
0.0064	-0.0030	0.0312	-0.0235	0.0106
-0.0124	0.0011	-0.0383	-0.0154	-0.0158
0.0000	0.0000	0.0000	0.0000	0.0000

G_{FL} =

14.2148	-87.3157
-116.8494	13.2775
-2.1579	-1.6464
-22.8541	-15.6222
0.0000	0.0000

B_{COL} =

-7.3162	-2.2816
0.9062	-0.2810
0.1303	1.4012
0.0000	0.0000

M_{OL} =

0.0000	1.0000	0.0000	0.0000
0.0000	0.0000	1.0000	0.0000
-0.0009	-0.0050	-0.0240	0.0000
-0.0001	0.0006	-0.9990	0.1070

N_{COL} =

0.0000	0.0000
0.0000	0.0000
-0.0110	0.1410
-0.0275	-0.0086

Angle of attack (ALPHA) = 60.0 (degrees)
Dynamic Pressure (QBAR) = 40.61 (psf)
Trim Velocity (VTOT) = 275.72 (ft/sec)

A_{OL} =

-0.0472	0.1523	-275.577	26.6070
-0.0058	-0.0638	0.2364	0.0000
0.0089	0.0320	-0.3957	0.0000
0.0000	1.0000	-0.6794	0.0000

B_{AP} =

-0.0156	0.0144	0.1020	0.2223	-0.0045
0.0051	-0.0022	0.0229	-0.0233	0.0104
-0.0131	-0.0001	-0.0298	-0.0127	-0.0145
0.0000	0.0000	0.0000	0.0000	0.0000

G_{FL} =

15.5391	-108.1458
-115.8728	16.6490
0.0000	0.0000
-23.7783	-13.3737
0.0000	0.0000

B_{COL} =

-7.1960	-1.0435
0.8933	-0.2756
0.1146	1.5810
0.0000	0.0000

M_{OL} =

0.0000	1.0000	0.0000	0.0000
0.0000	0.0000	1.0000	0.0000
-0.0013	-0.0083	-0.0097	0.0000
-0.0002	0.0006	-0.9995	0.0965

N_{COL} =

0.0000	0.0000
0.0000	0.0000
-0.0029	0.1866
-0.0261	-0.0038

REFERENCES

Aeronautical Systems Division, Air Force Systems Command 1990: *Military Specification - Flying Qualities of Piloted Vehicles*. MIL-STD-1797A.

Ashworth, B.R.; and Kahlbaum, W.M., Jr. 1973: *Description and Performance of the Langley Differential Maneuvering Simulator*. NASA TN D-7304.

Bowers, A.H.; Noffz, G.K.; Grafton, S.B.; Mason, M.L.; and Peron, L.R. 1990: *Multiaxis Thrust Vectoring Using Axisymmetric Nozzles and Postexit Vanes on an F/A-18 Configuration Vehicle*. NASA CP-3149 Volume 1, Part 2.

Bundick, W.T.; Pahle, J.W.; Yeager, J.C.; and Beissner, F.L. 1996: *Design of a Mixer for the Thrust-Vectoring System on the High-Alpha Research Vehicle*. NASA TM-110228.

Buttrill, C.S.; Arbuckle, P.D.; and Hoffler, K.D. 1992: *Simulation Model of a Twin-Tail, High Performance Airplane*. NASA TM-107601.

Cooper, G.E.; and Harper, R.P., Jr. 1969: *The Use of Pilot Rating in the Evaluation of Aircraft Handling Qualities*. NASA TN D-5253.

Davidson, J.B.; and Schmidt, D.K. 1986: *Flight Control Synthesis For Flexible Aircraft Using Eigenspace Assignment*. NASA CR-178164.

Davidson, J.B.; Foster, J.V.; Ostroff, A.J.; Lallman, F.J.; Murphy, P.C.; Hoffler, K.D.; and Messina, M.D. 1992: *Development of a Control Law Design Process Utilizing Advanced Synthesis Methods with Application to the NASA F-18 HARV*. NASA CP-3137, Volume 4, pp. 111-157.

Doane, P.M.; Gay, C.H.; Fligg, J.A.; et al. 1990: *Multi-System Integrated Control (MuSIC) Program*. WRDC-TR-90-6001.

Fears, S.; Hoffler, K.D.; and Carzoo, S. 1997: *Piloted Simulator Study of the Effectiveness of a Series of Agile Fighter Aircraft Armed with High-Off-Boresight Missiles and Helmet-Mounted Sights During 1-Versus-1 and 1-Versus-2 Close-In Air Combat Engagements*, NASA CR-201652.

Foster, J.V.; Bundick, W.T.; and Pahle, J.W. 1991: Controls for Agility Research in the NASA High-Alpha Technology Program. SAE Paper No. 912148, September.

Gilbert, W.P.; and Gatlin, D.H. 1990: Review of the NASA High-Alpha Technology Program. *High Angle-of-Attack Technology-Volume 1*. NASA CP-3149, Part 1, pp. 23-59.

Hamilton, W.L.; and Skow, A. M. 1984: *Operational Utility Survey: Supermaneuverability*. AFWAL-TR-85-3020.

HARV Control Law Design Team 1996: *Design Specification for a Thrust-Vectoring, Actuated-Nose-Strake Flight Control Law for the High-Alpha Research Vehicle*. NASA TM-110217.

Herbst, W.B.; and Krogull, B. 1972: Design for Air Combat. AIAA Paper 72-749, August.

Herbst, W.B. 1980: Future Fighter Technologies. *Journal of Aircraft*, Volume 17, Number 8, August.

Hoffler, K.D.; Brown, P.W.; Phillips, M.R.; Rivers, R.A.; Davidson, J.B.; Lallman, F.J.; Murphy, P.C.; and Ostroff, A.J. 1994: Evaluation Maneuver and Guideline Development For High-Alpha Control Law Design Using Piloted Simulation. AIAA Paper No. 94-3512, August.

Lallman, F.J. 1985: *Relative Control Effectiveness Technique With Application to Airplane Control Coordination*. NASA TP-2416.

Lallman, F.J.; Davidson, J.B.; and Murphy, P.C. 1998: *A Method for Integrating Thrust-Vectoring and Actuated Forebody Strakes with Conventional Aerodynamic Controls on a High-Performance Fighter Airplane*. NASA/TP-1998-208464.

Mason, M.L.; Capone, F.J.; and Asbury, S.C. 1992: *A Static Investigation of the F/A-18 High-Alpha Research Vehicle Thrust Vectoring System*. NASA TM-4359.

Moorhouse, D.J.; and Moran, W. A. 1985: Flying Qualities Design Criteria For Highly Augmented Systems. *Proceedings, IEEE National Aerospace and Electronics Conference*, NAECON, May 20-24.

Murphy, P.C.; and Davidson, J.B. 1991: Control Design for Futu e Agile Fighters. AIAA Paper No. 91-2882, August.

Murphy, P.C.; Hoffler, K.D.; Davidson, J.B.; Ostroff, A.J.; Lallman, F.J.; and Messina, M.D. 1994: Preliminary Evaluation of HARV NASA-1 Control Law Flight Test Results. *Proceedings, Fourth High Alpha Conference*, NASA Dryden Flight Research Center, NASA CP-10143, July 12-14.

Murphy, P.C.; and Davidson, J.B. 1998: A Control Law Design Method Facilitating Control Power, Robustness, Agility, and Flying Qualities Tradeoffs: CRAFT. NASA/TP-1998-208463.

Ogburn, M.E.; Nguyen, L.T.; Wunschel, A.J.; Brown, P.W.; and Carzoo, S.W. 1988: *Simulation Study of Flight Dynamics of a Fighter Configuration With Thrust-Vectoring Controls at Low Speeds and High Angles of Attack*. NASA TP-2750.

Ostroff, A.J.; and Proffitt, M.S. 1993: *Longitudinal-Control Design Approach for High-Angle-of-Attack Aircraft*. NASA TP-3302.

Ostroff, A.J.; Hoffler, K.D.; and Proffitt, M.S. 1994: *High-Alpha Research Vehicle (HARV) Longitudinal Controller: Design, Analyses, and Simulation Results*. NASA TP-3446.

Srinathkumar, S. 1978: *Eigenvalue/Eigenvector Assignment Using Output Feedback*. NASA TP-1118.

Wilson, D.J.; Riley, D.R.; and Citurs, K.D. 1993a: *Aircraft Maneuvers for the Evaluation of Flying Qualities and Agility -Maneuver Descriptions and Selection Guide*. WL-TR-93-3082.

Wilson, D.J.; Riley, D.R.; and Citurs, K.D. 1993b: *Flying Qualities Criteria Development Through Manned Simulation for 60° Angle of Attack - Final Report : Volume 1 and 2*. NASA CR-4535.

Wilson, D.J.; and Citurs, K.D. 1996: *High Angle of Attack Flying Qualities Design Guidelines : Volume 1 and 2*. NASA CR-4681.

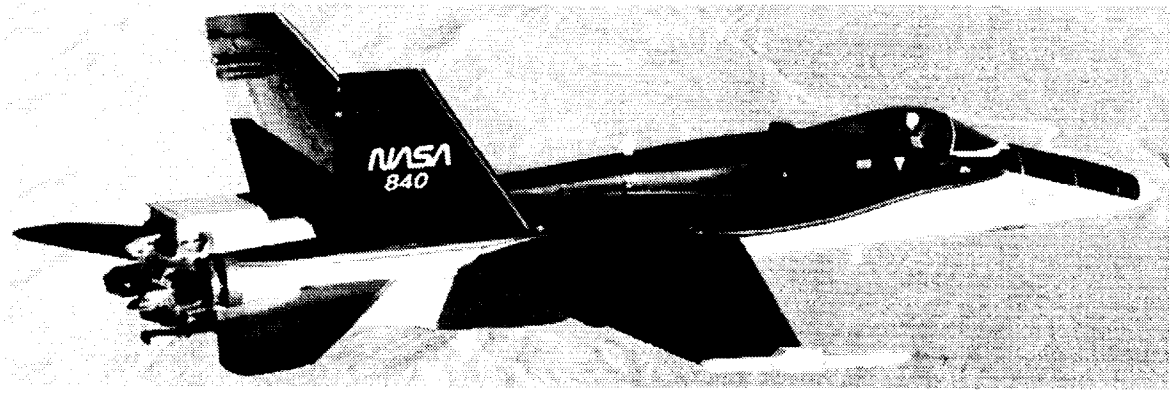

(a) HARV in flight.

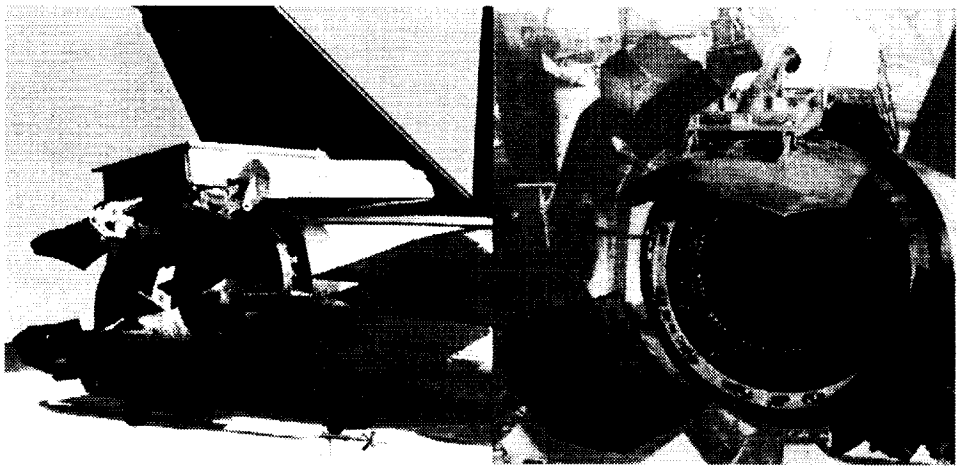

(b) Close-up of thrust vectoring apparatus.

Figure 1. High-Alpha Research Vehicle (HARV).

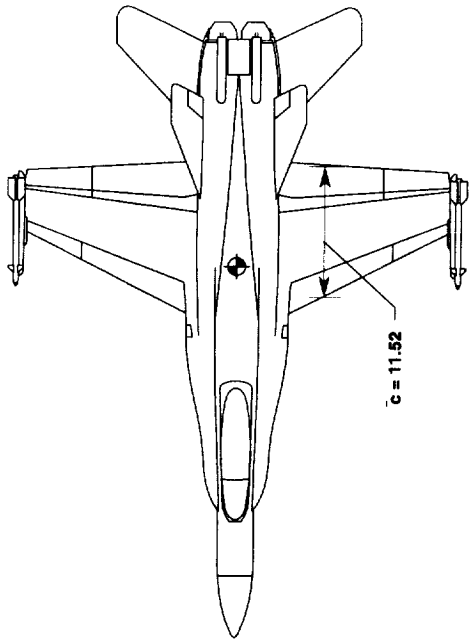

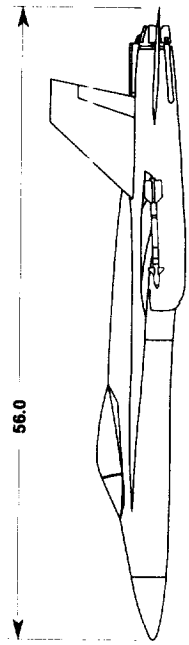

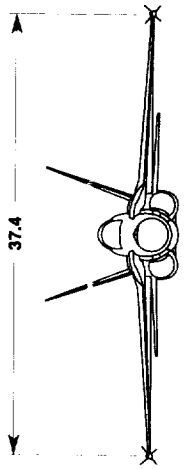

Figure 2. Major dimensions (feet) of the HARV.

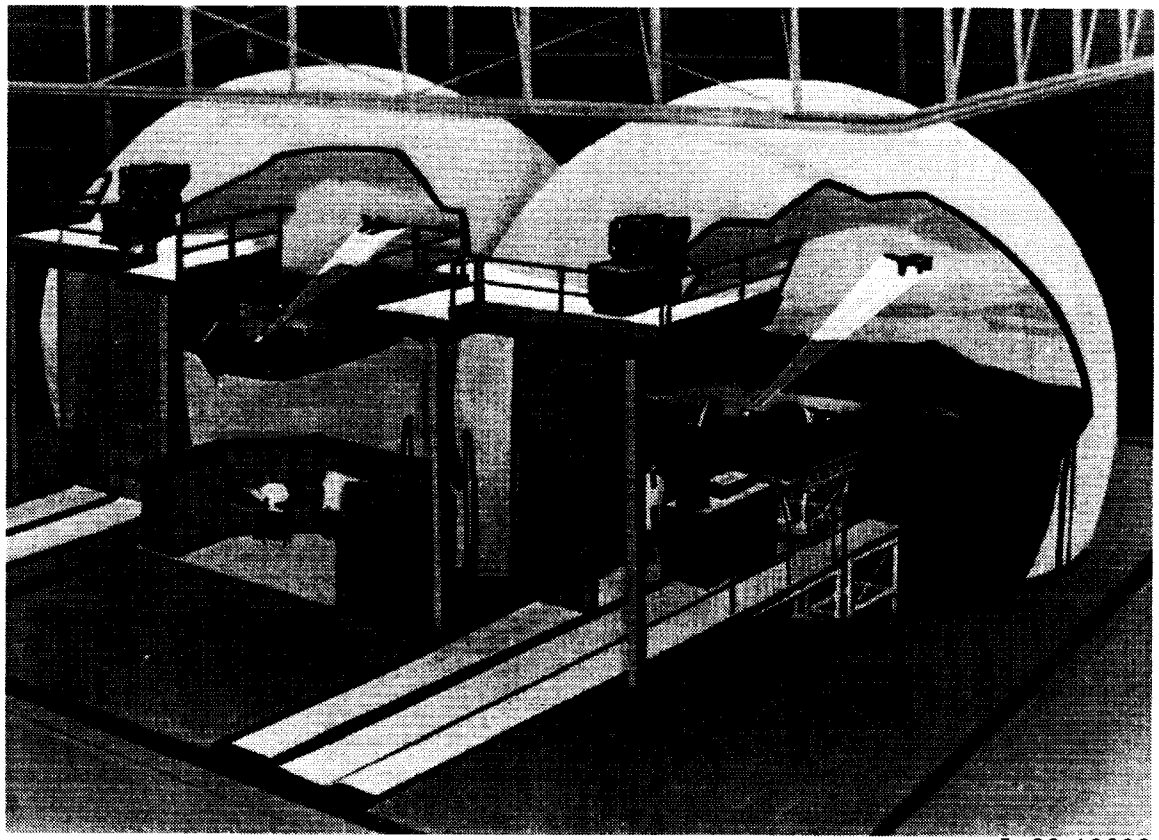

L-90-10308

Figure 3. NASA Differential Maneuvering Simulator (DMS).

L-90-5138

Figure 4. Photo of Differential Maneuvering Simulator (DMS) cockpit.

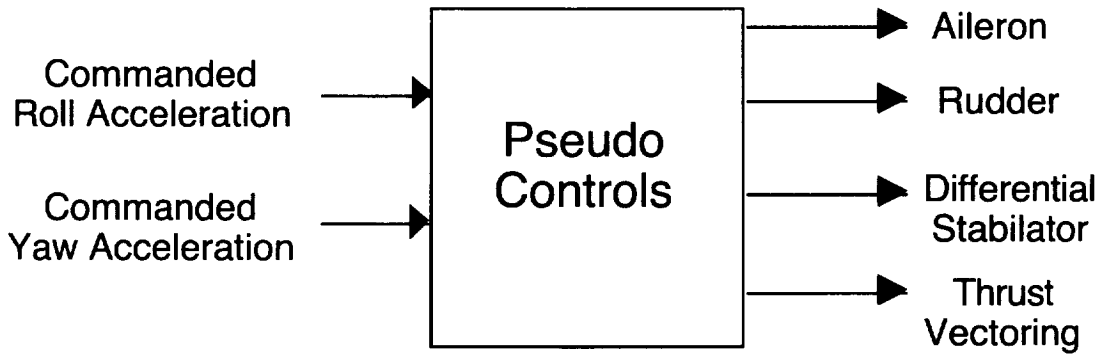

Figure 5. Pseudo Controls.

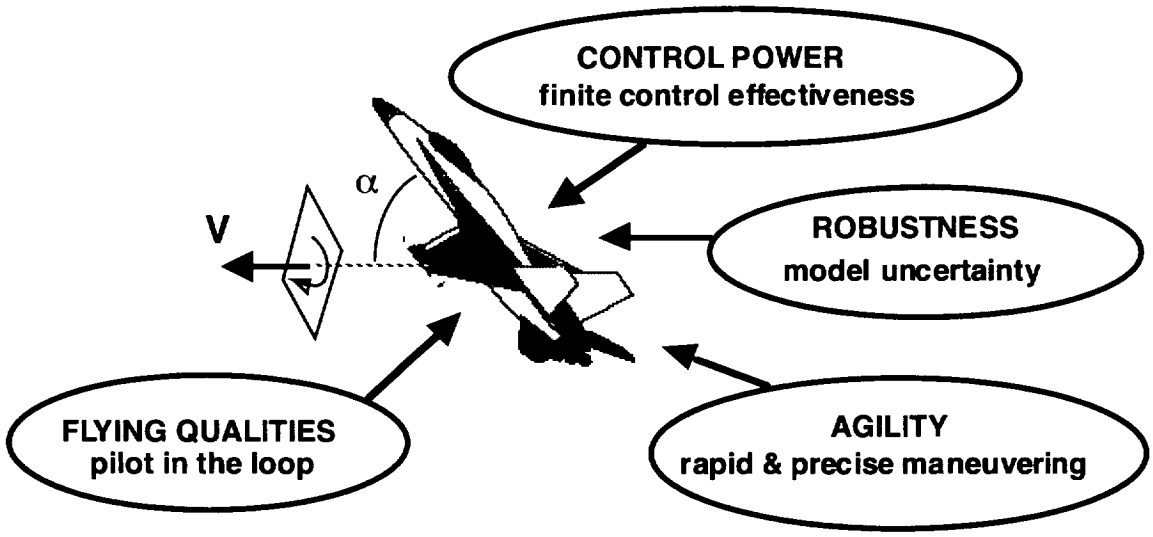

Figure 6. CRAFT tradeoffs.

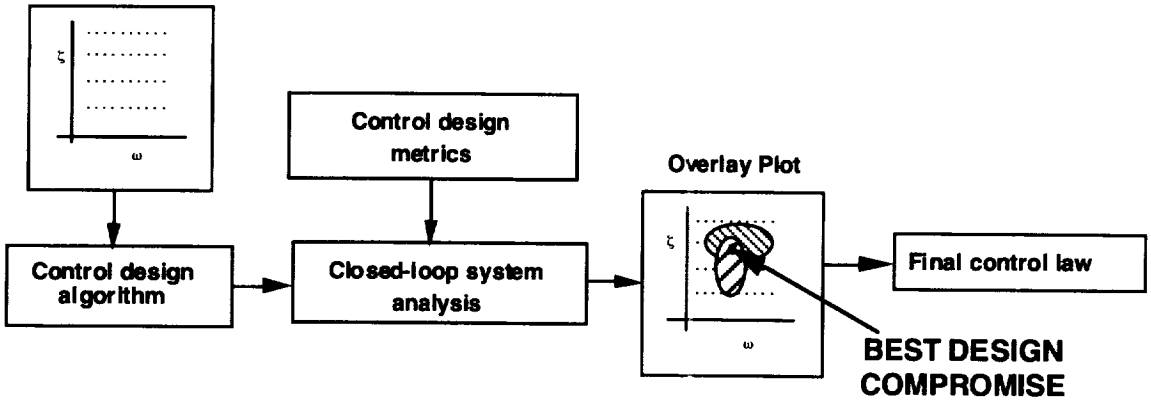

Figure 7. CRAFT design process.

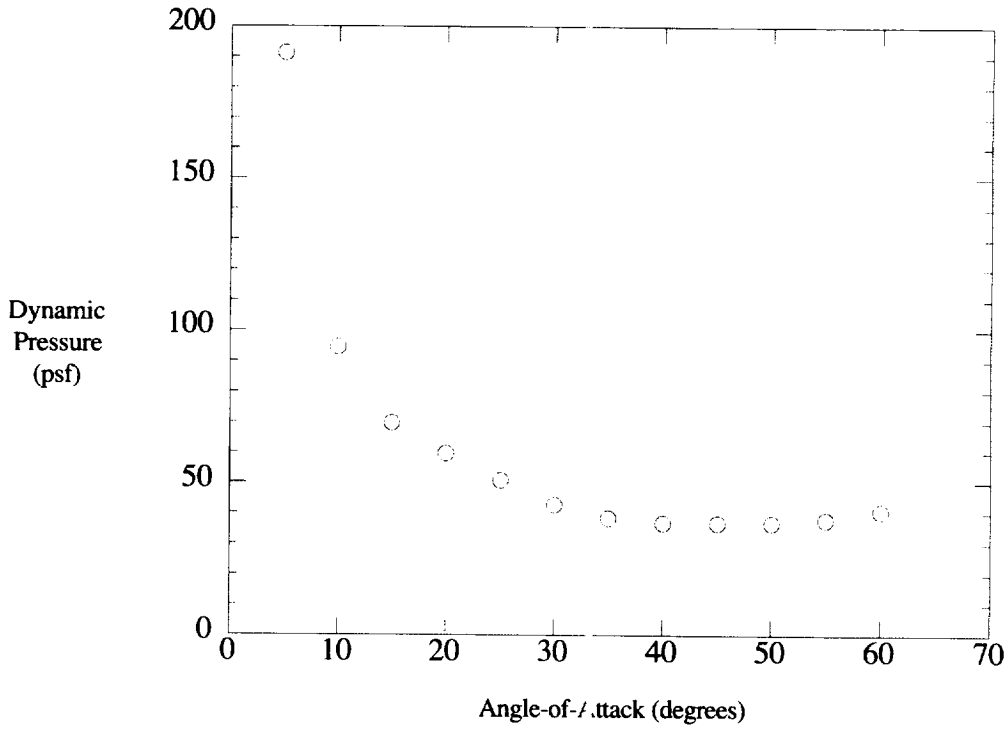

Figure 8. Design conditions - dynamic pressure versus angle-of-attack.

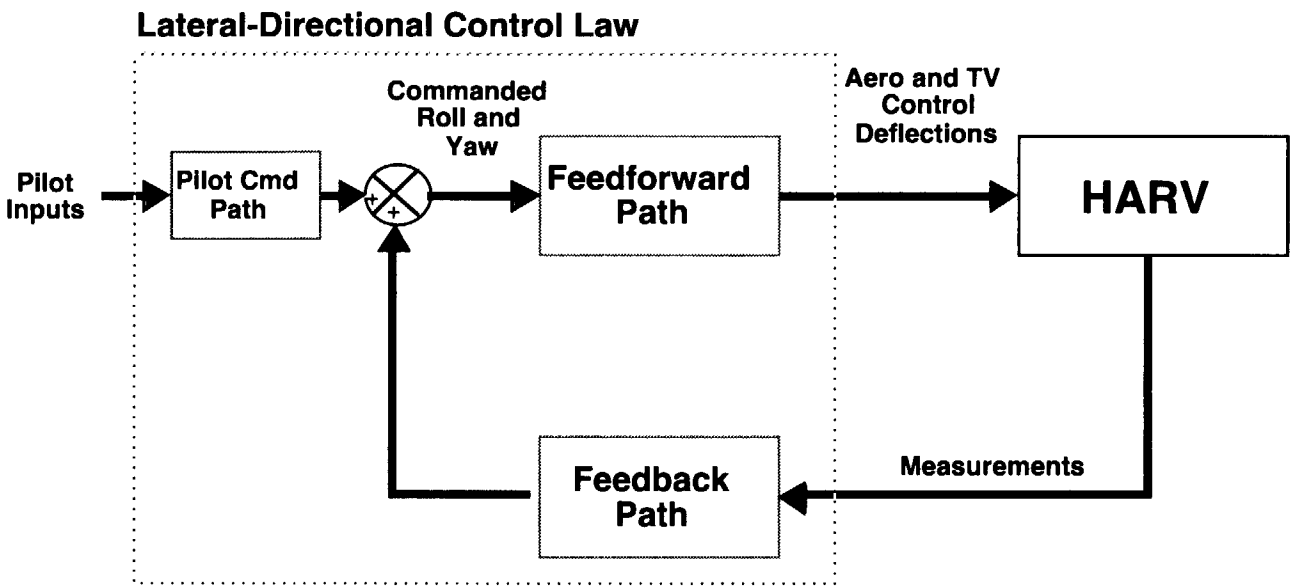

Figure 9. Control law overview.

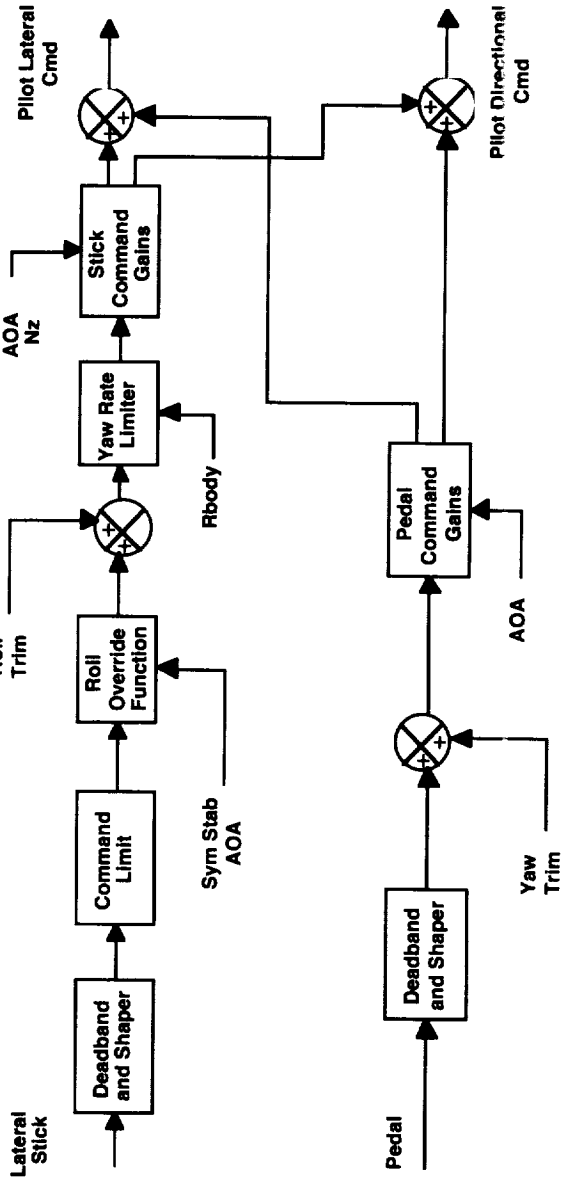

Figure 10a. Pilot command path.

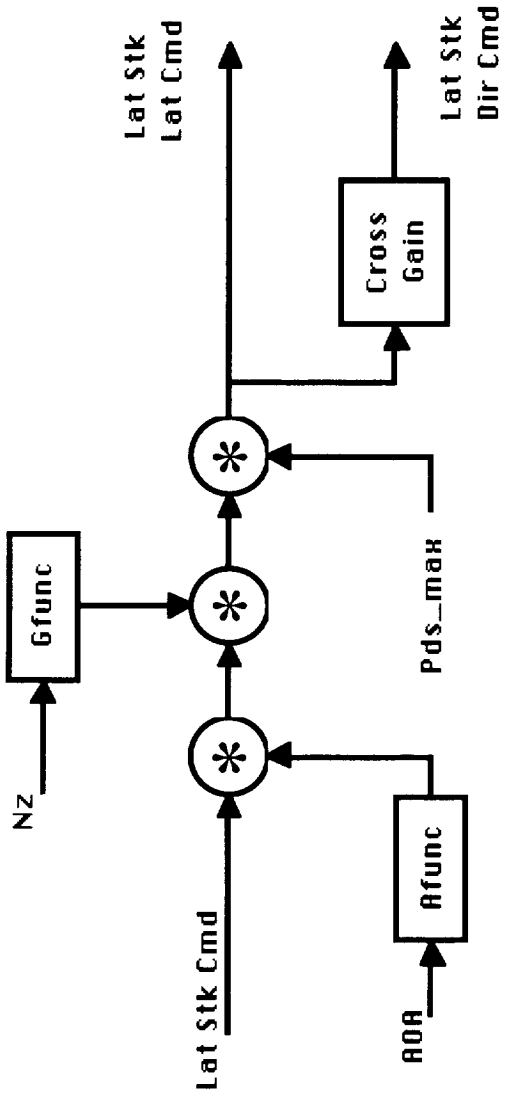

Figure 10b. Lateral stick command gain element.

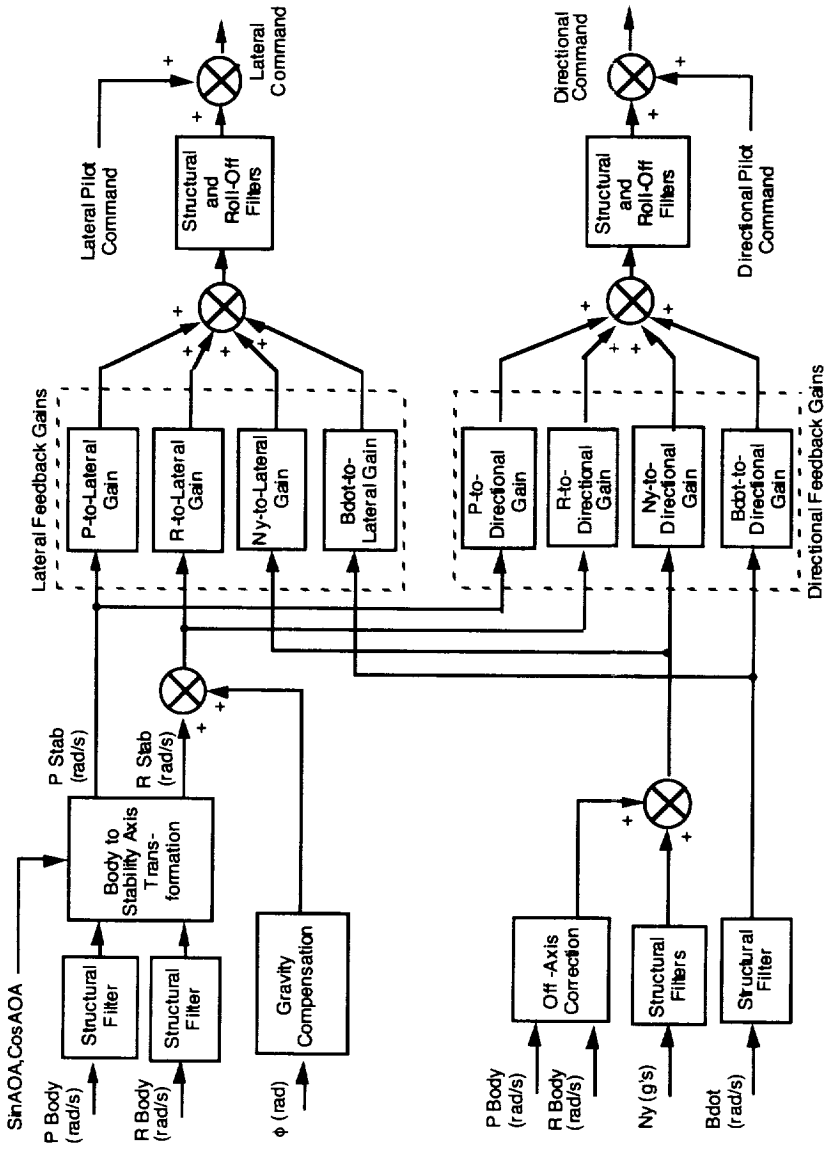

Figure 11. Feedback path.

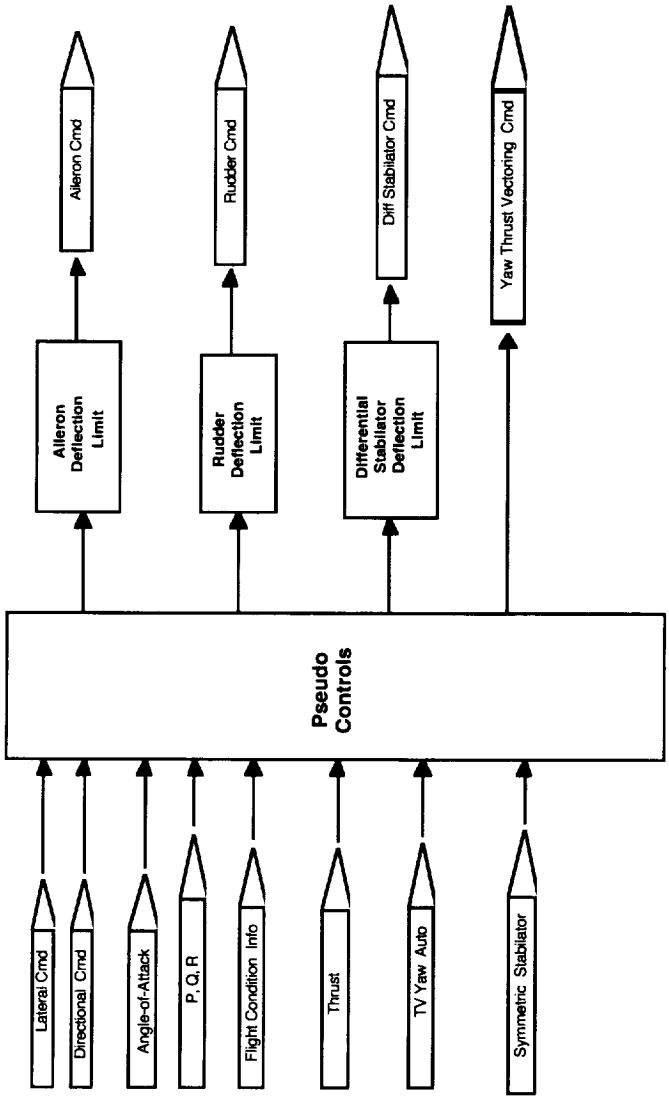

Figure 12. Feedforward path.

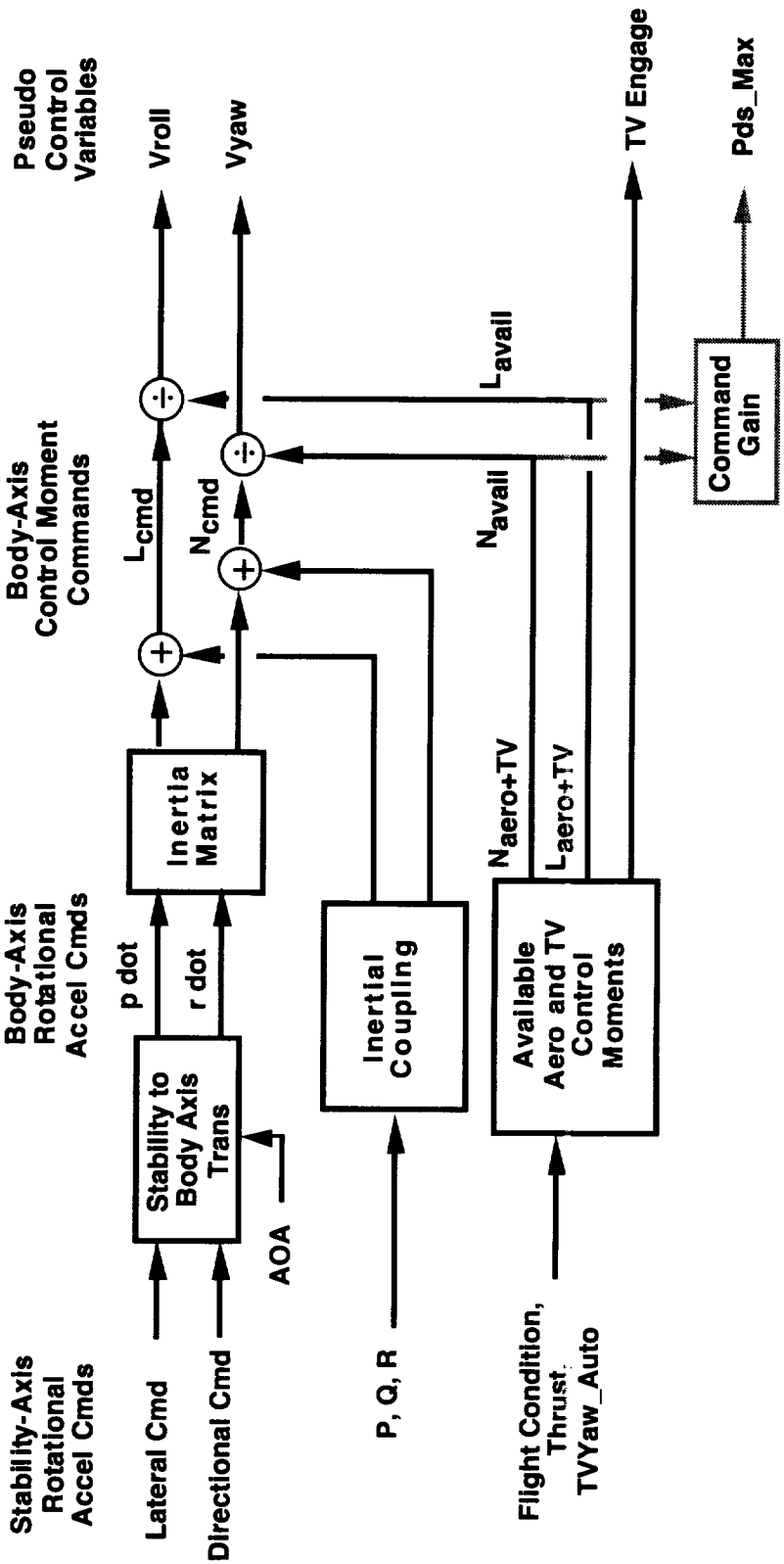

Figure 13. Feedforward interconnect.

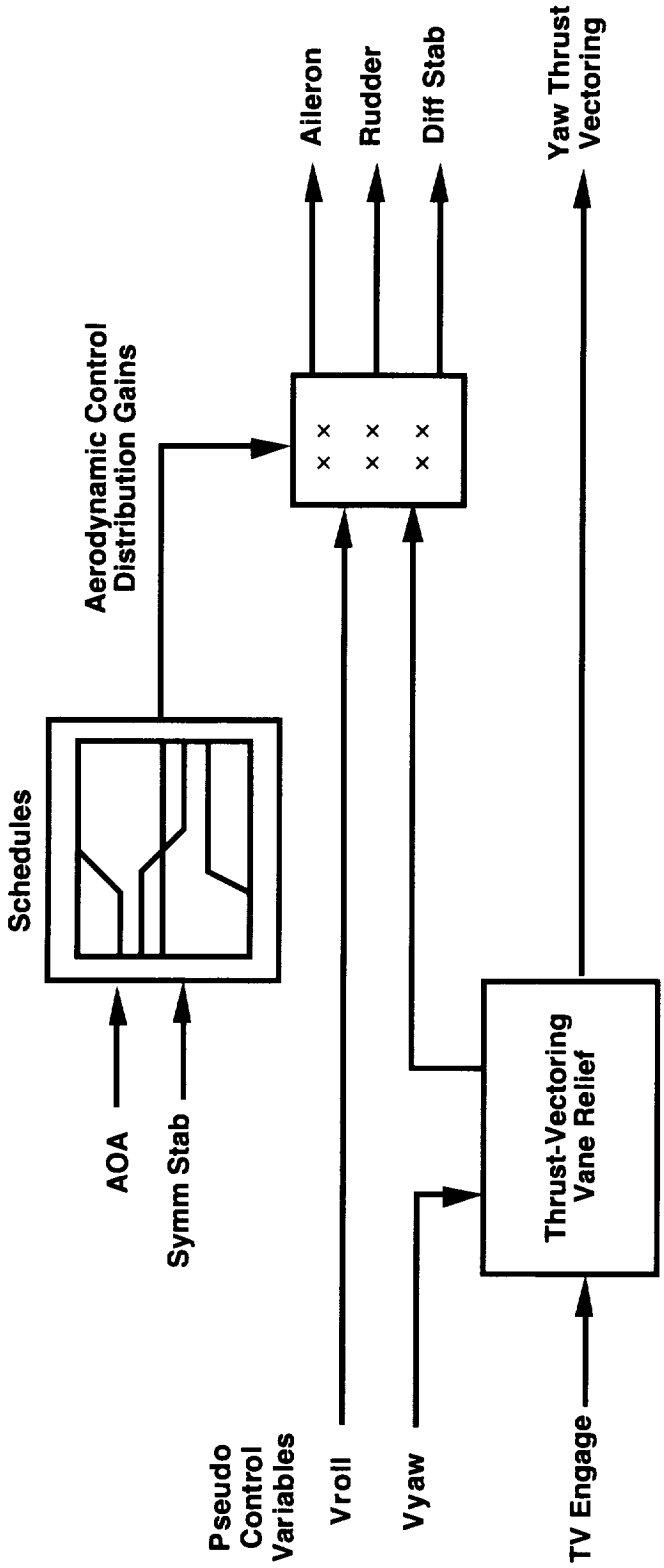

Figure 14. Feedforward distributor.

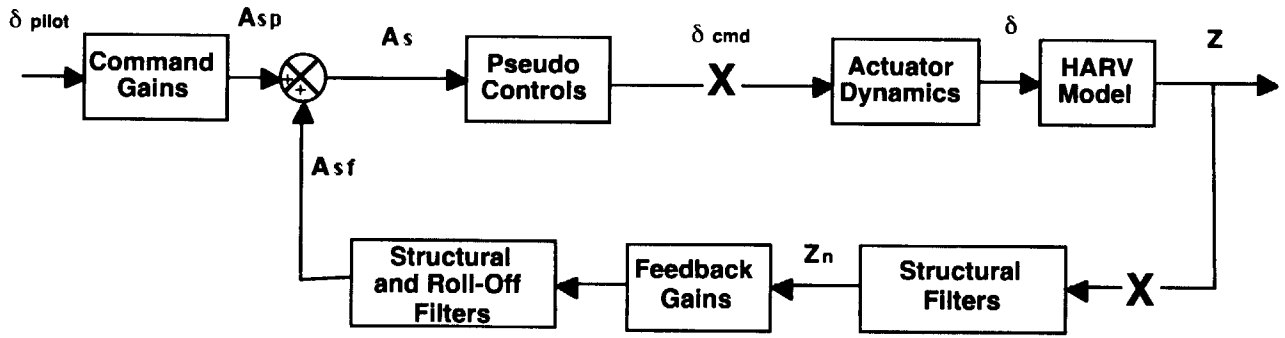

X - denotes where loop is broken for analysis

Figure 15. Gain and phase margin analysis.

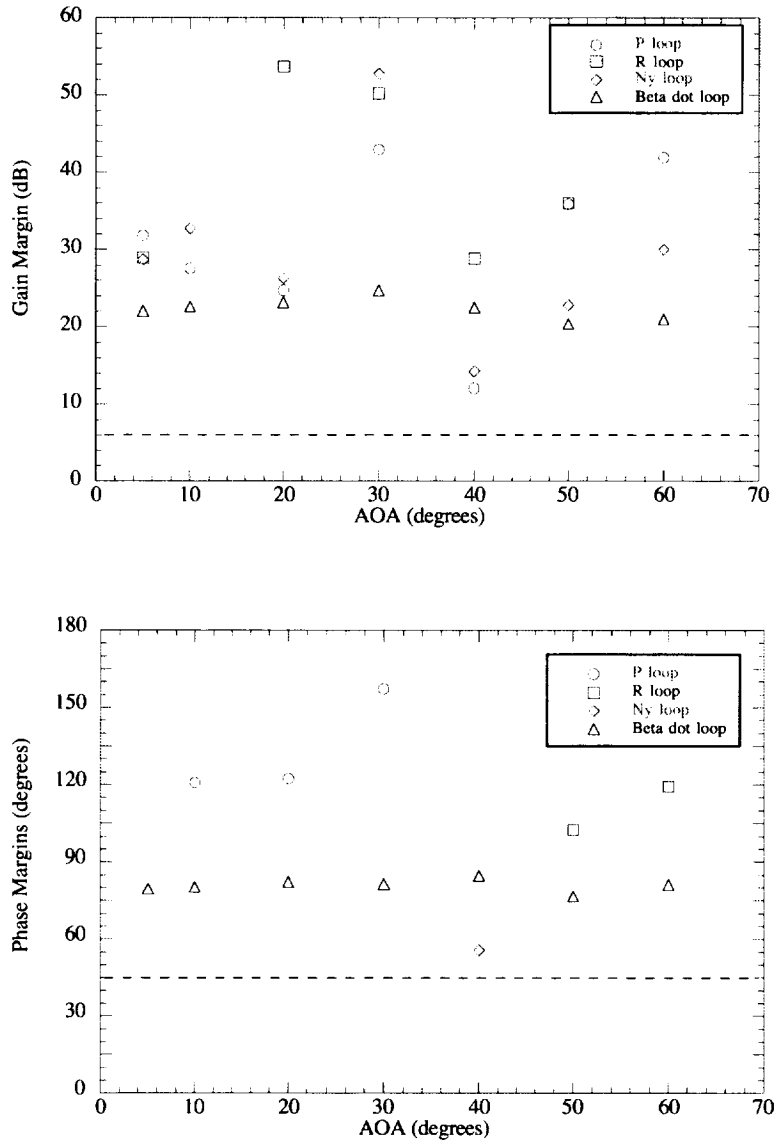

Figure 16. Single loop gain and phase margins for measurement loops at 15 000, 25 000, and 35 000 feet, at 1*g*.

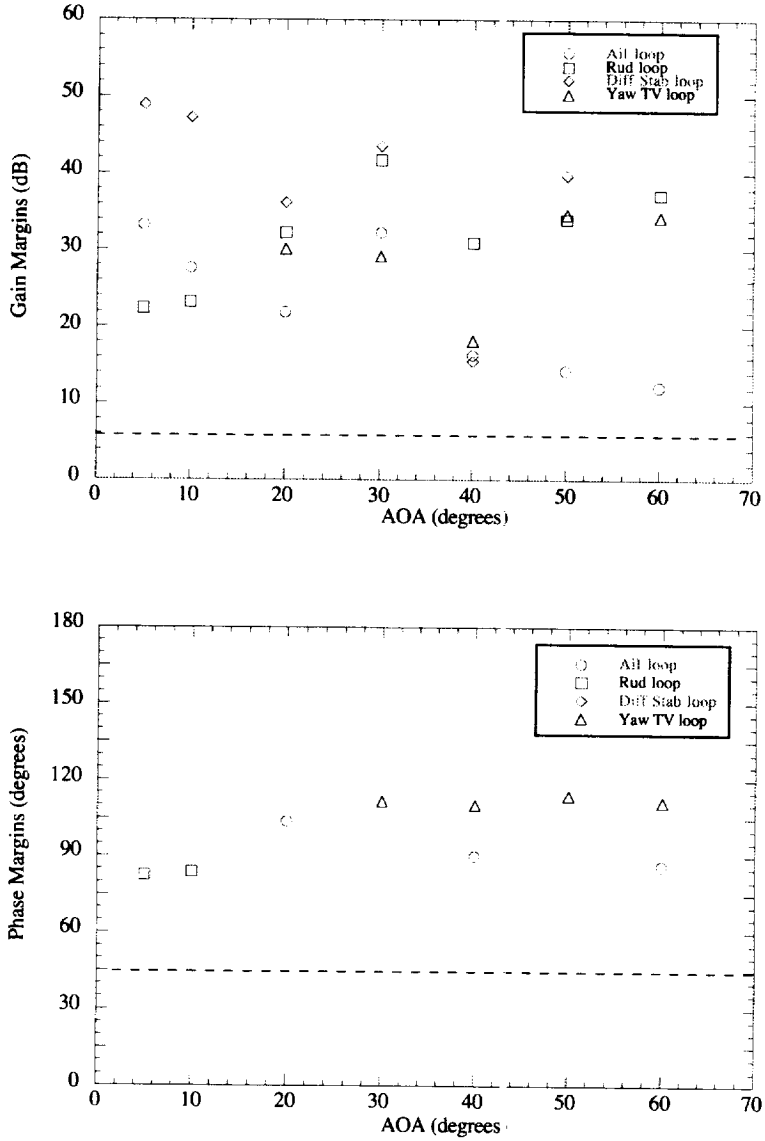

Figure 17. Single loop gain and phase margins for actuator commands at $1g$, $2g$, and $4g$ at 25 000 feet.

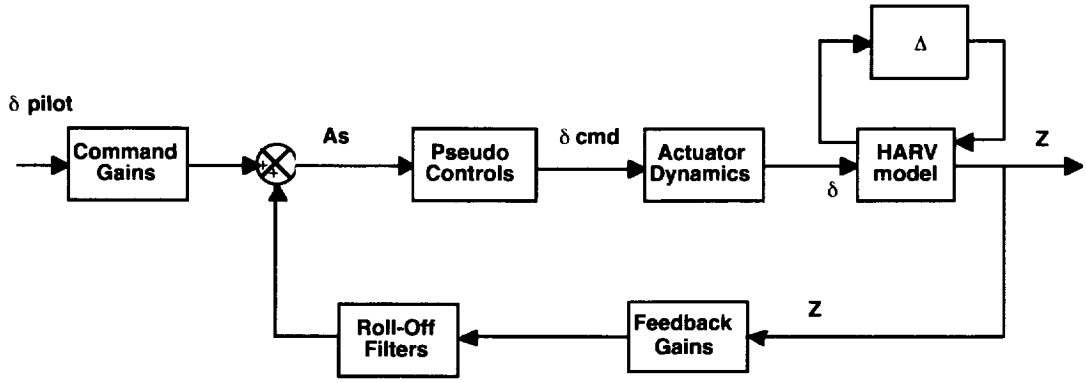

Figure 18. Structured singular value analysis.

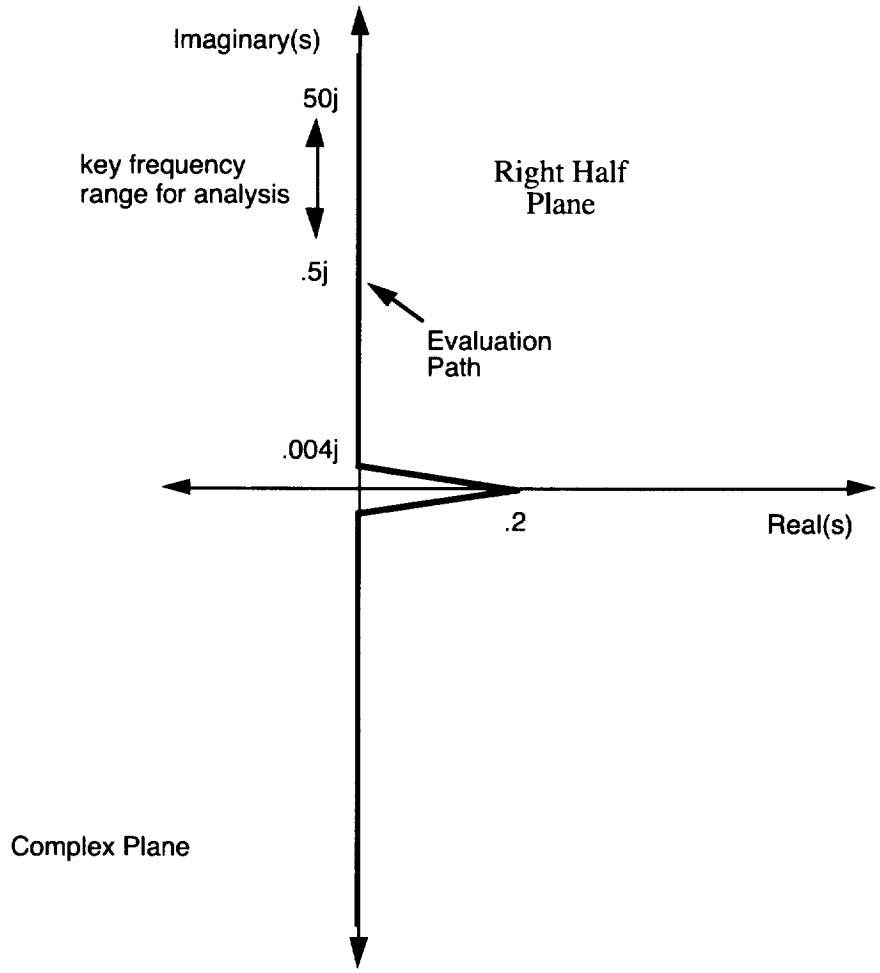

Figure 19. Modified evaluation path for real structured singular value stability robustness analysis test.

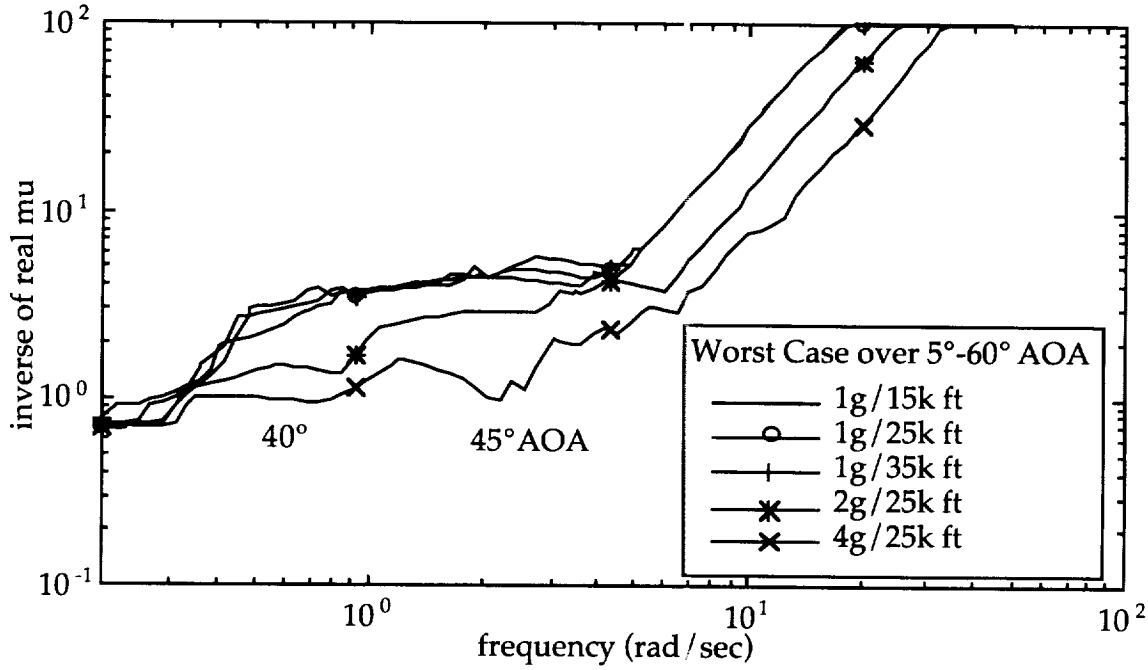

Figure 20. Worst case $(\mu_R)^{-1}$ over angle of attack corresponding to simultaneous real variations of stability derivatives: Y_v, N_v, L_p, and N_r.

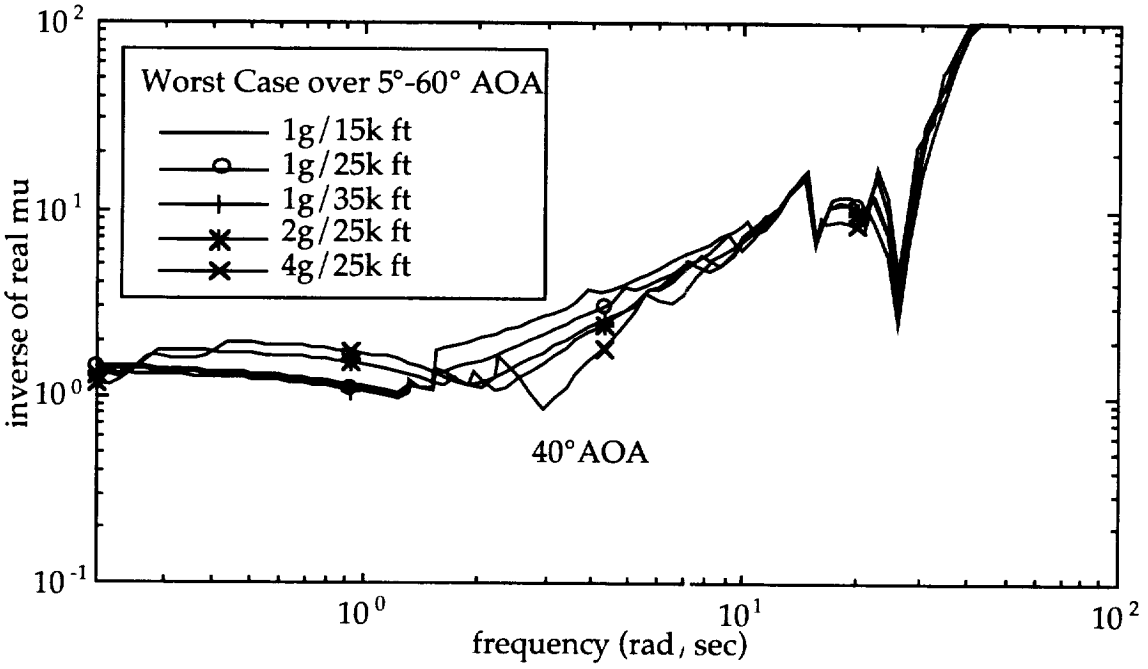

Figure 21. Worst case $(\mu_R)^{-1}$ over angle of attack corresponding to simultaneous real variations of control derivatives: L_{ail}, N_{rud}, L_{dstab}, and N_{yjet}.

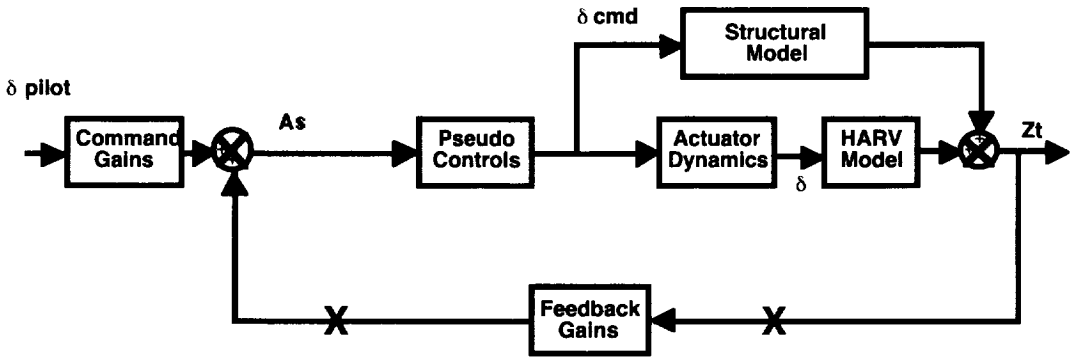

x - denotes where loop is broken for analysis

Figure 22. Servo-elastic analysis.

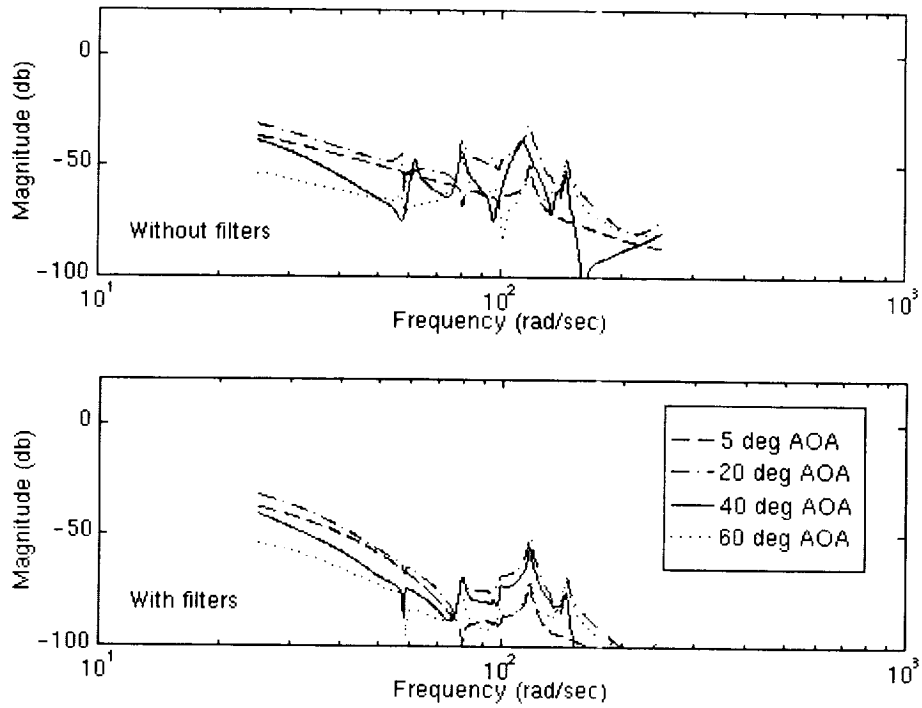

Figure 23. P loop broken - without and with structural filters.

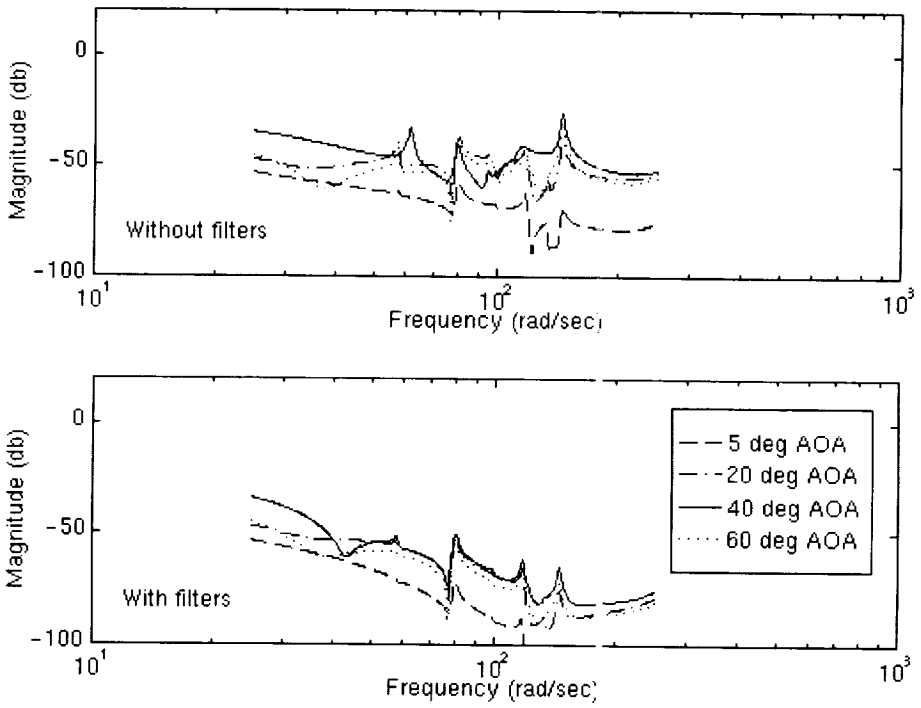

Figure 24. R loop broken - without and wi h structural filters.

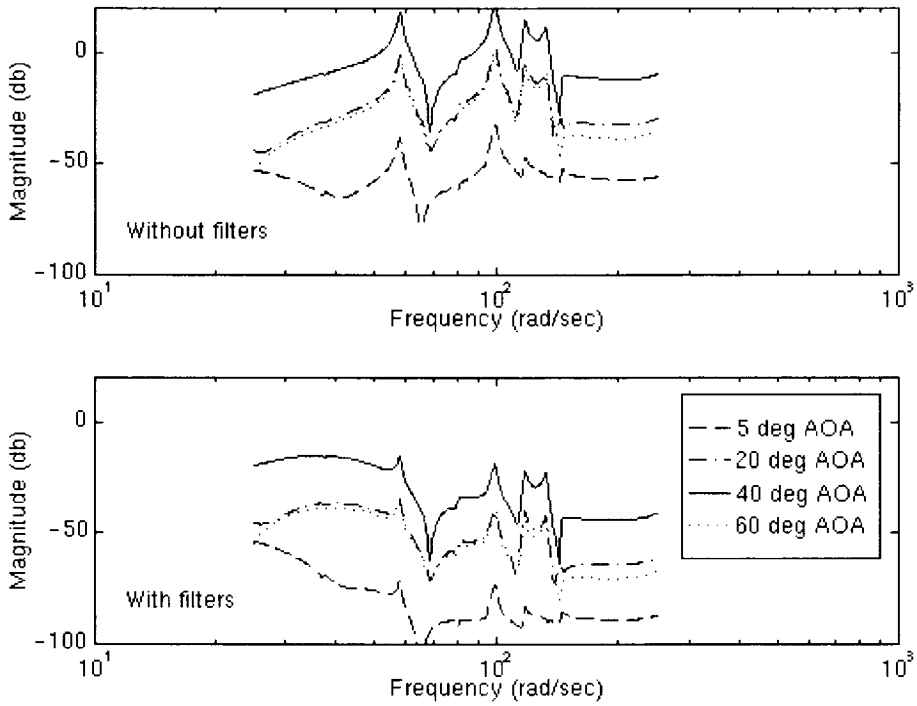

Figure 25. Ny loop broken - without and with structural filters.

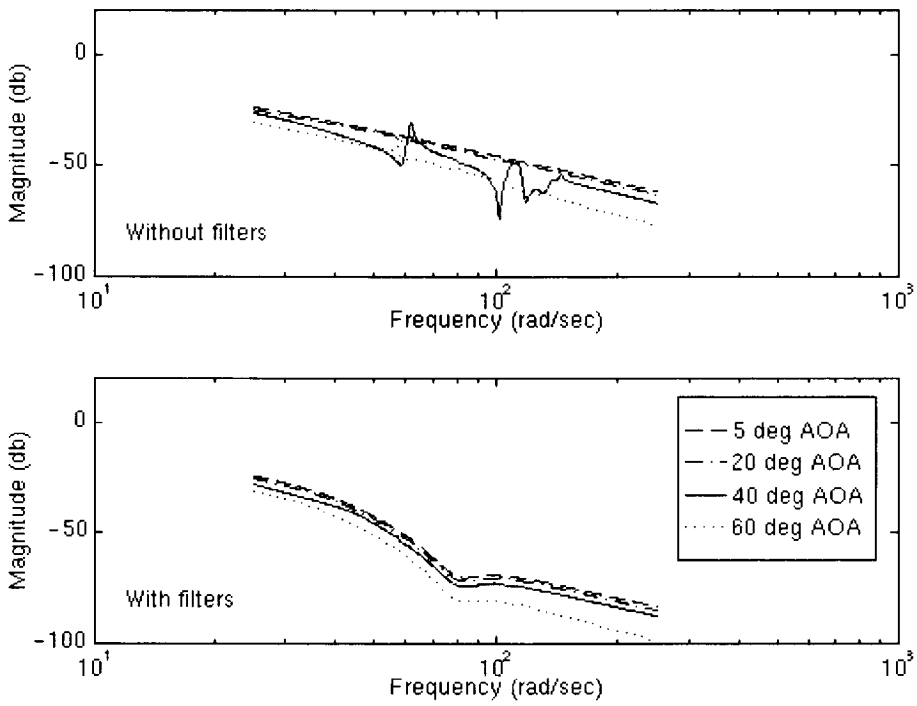

Figure 26. Beta dot loop broken - without and with structural filters.

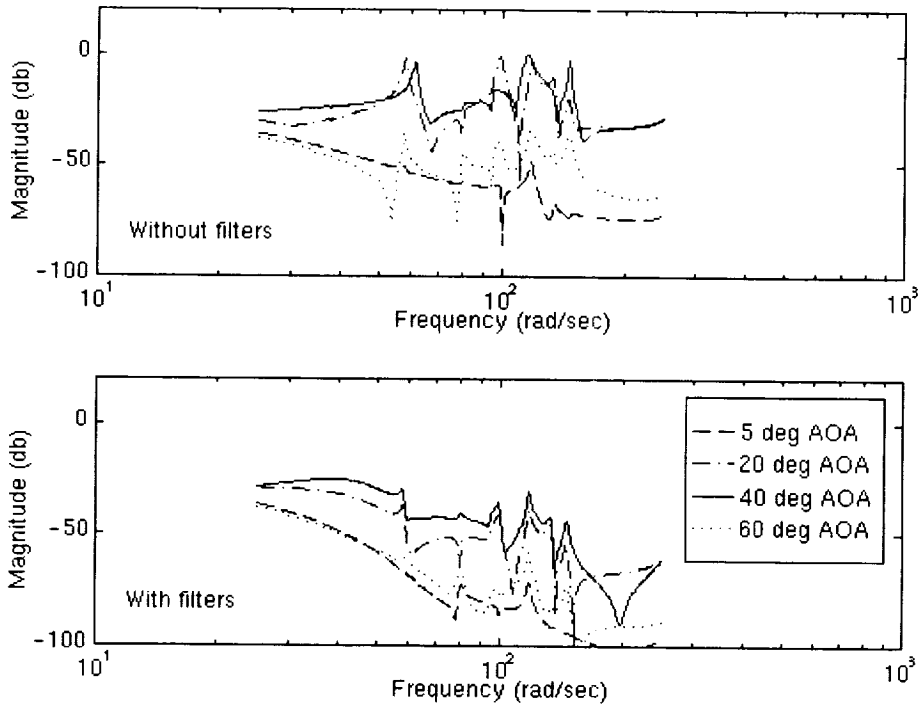

Figure 27. Roll acceleration command loop broken - without and with structural filters.

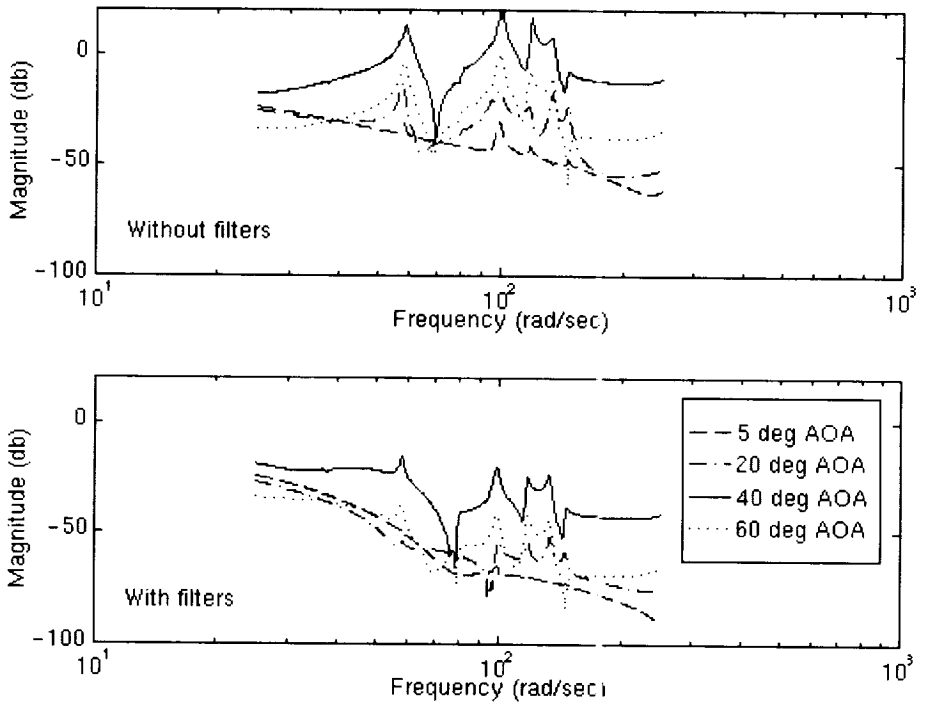

Figure 28. Yaw acceleration command loop broken - w thout and with structural filters.

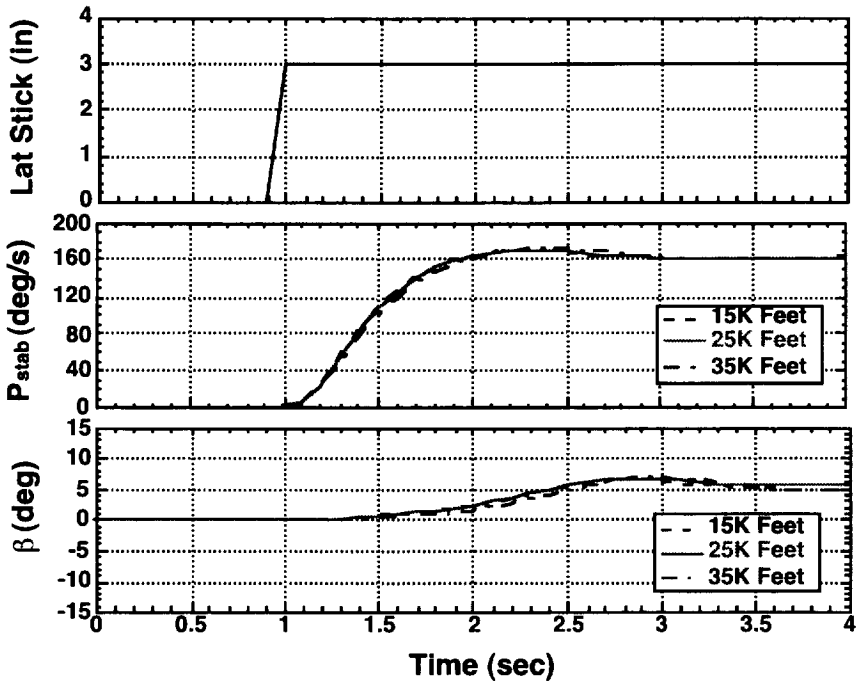

Figure 29. Maximum lateral stick step time responses for 5 degrees angle-of-attack at 15 000, 25 000, and 35 000 feet at 1g.

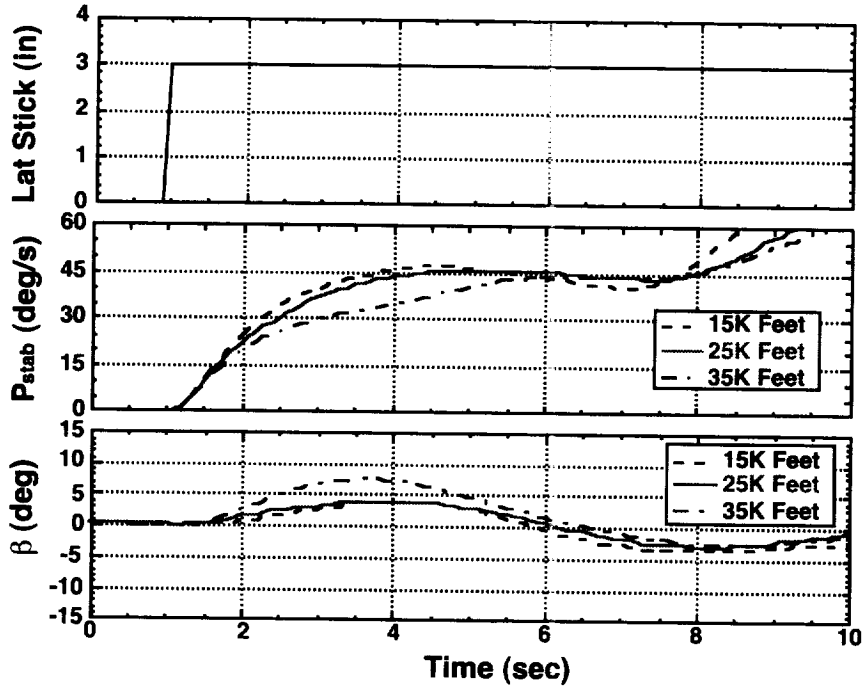

Figure 30. Maximum lateral stick step time responses for 35 degrees angle-of-attack at 15 000, 25 000, and 35 000 feet at $1g$.

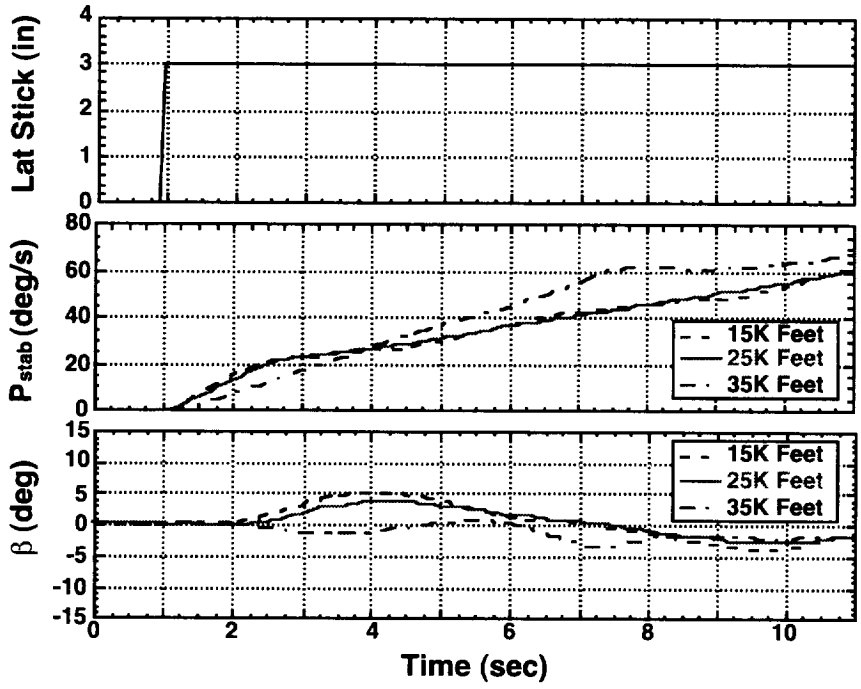

Figure 31. Maximum lateral stick step time responses for 60 degrees angle-of-attack at 15 000, 25 000, and 35 000 feet at $1g$.

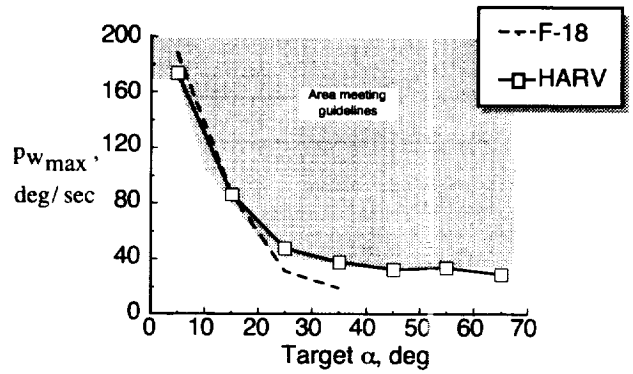

Figure 32. Maximum wind-axis roll rate achieved with maximum lateral stick before reaching wind-axis bank angle change of 90° from 1g at 25 000 feet.

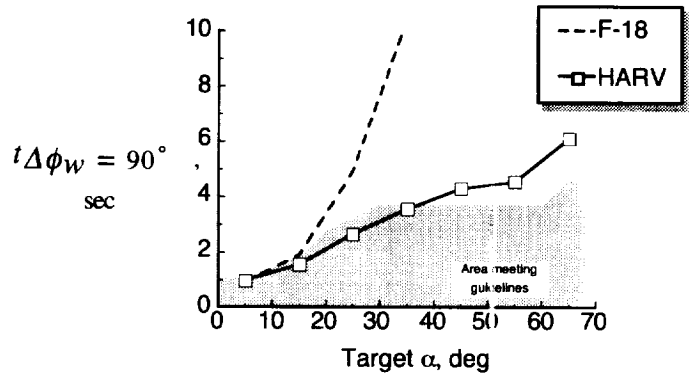

Figure 33. Time to bank through a wind-axis bank angle change of 90° from 1g at 25 000 feet.

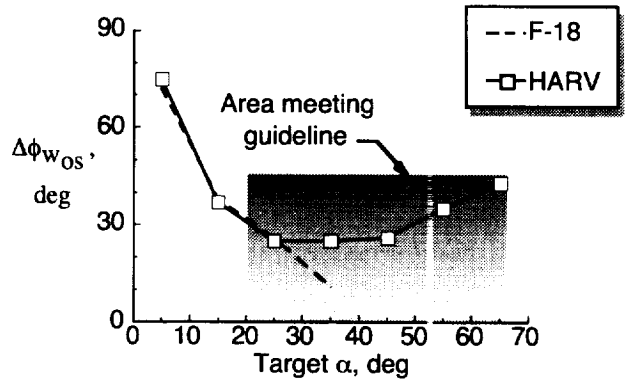

Figure 34. Wind-axis bank angle overshoot from stick reversal after 90° of wind-axis bank angle change.

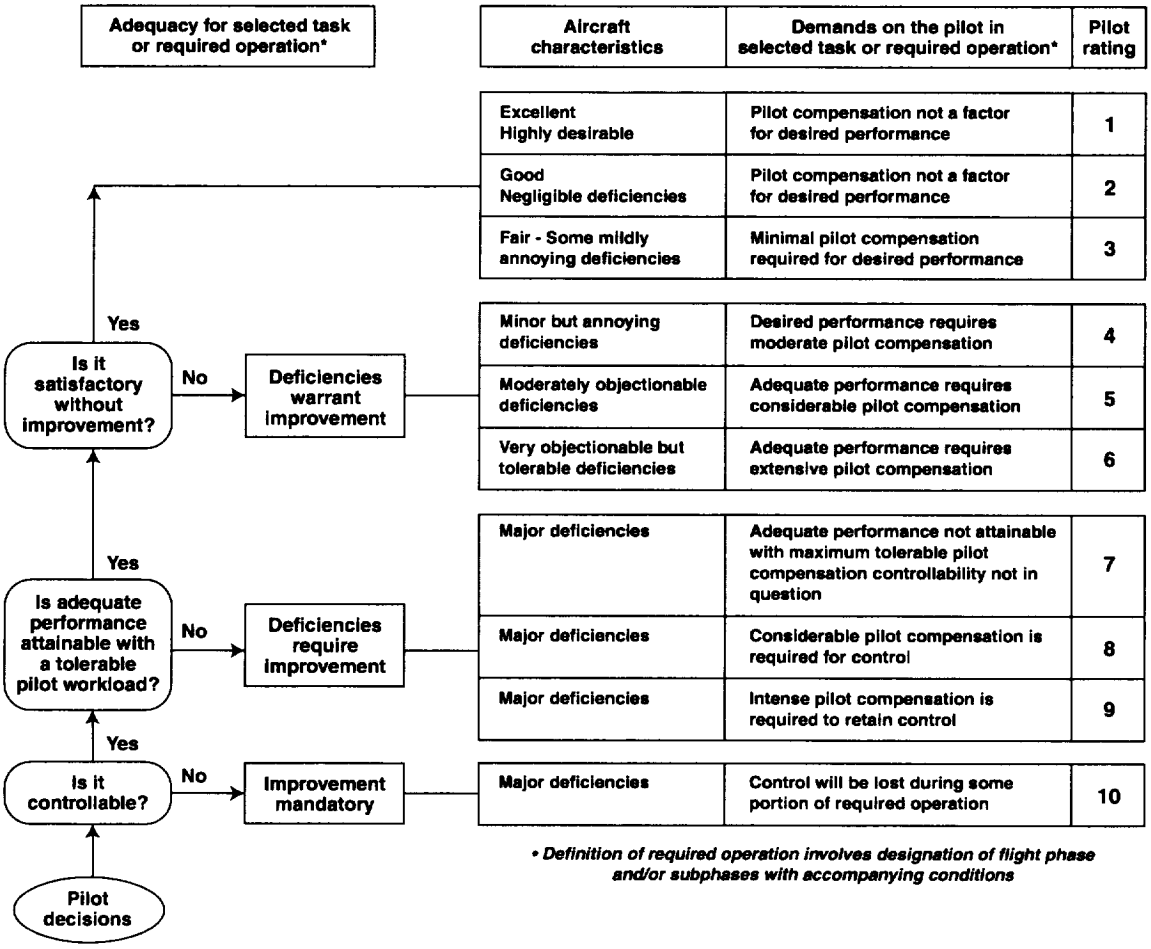

Figure 35. Cooper-Harper handling qualities rating scale (Cooper and Harper 1962).

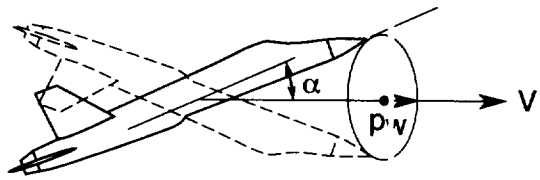

$$p_w = p\cos(\alpha) + r\sin(\alpha)$$

Figure 36. Coning motion during high-angle-of-attack rolls.

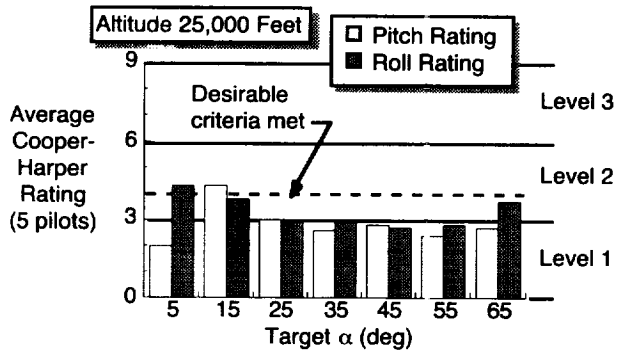

Figure 37. Average CHR's for 1g 360° roll maneuver.

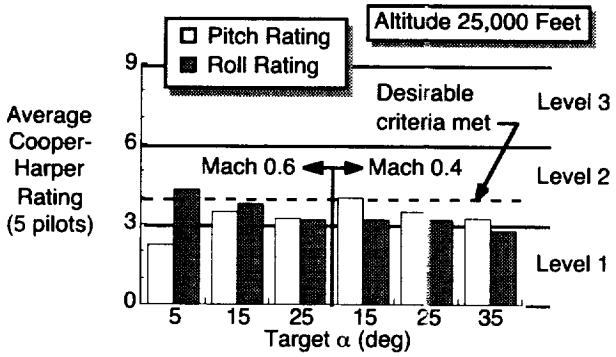

Figure 38. Average CHR's for loaded roll maneuver.

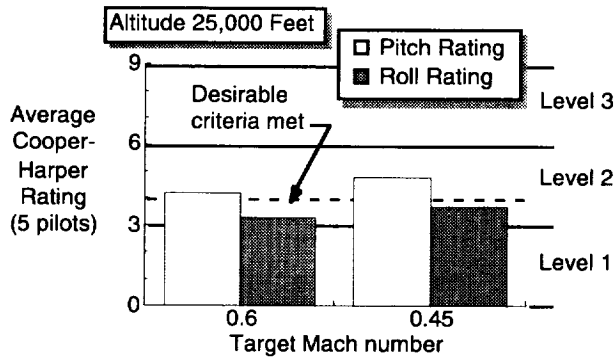

Figure 39. Average CHR's for $3g$ tracking task maneuver.

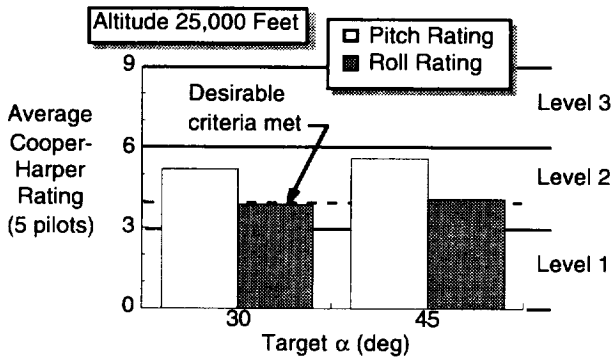

Figure 40. Average CHR's for high-α tracking tasks.

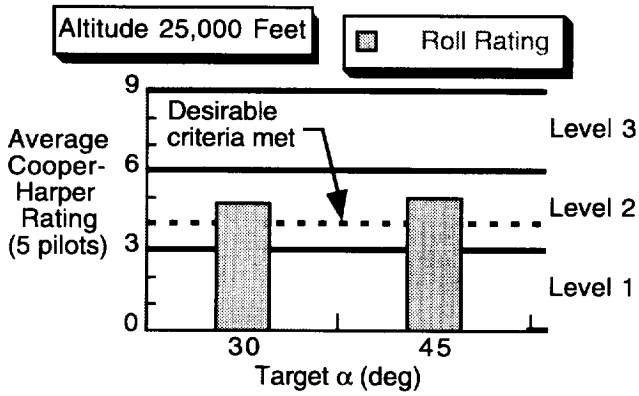

Figure 41. Average CHR's for high-α target acquisition tasks.

Table 1. Control Surface Position and Rate Limits

Surface	Position Limit (deg)	Rate Limit (deg/sec)
Stabilator		40
Trailing Edge Up	24	
Trailing Edge Down	10.5	
Aileron		100
Trailing Edge Up	25	
Trailing Edge Down	45	
Rudder		82
Trailing Edge Left	30	
Trailing Edge Right	30	
Trailing Edge Flap		18
Trailing Edge Up	8	
Trailing Edge Down	45	
Leading Edge Flap		15
Leading Edge Up	3	
Leading Edge Down	33	
Speed Brake		~20 to 30
Trailing Edge Up	60	

Table 2. Physical Characteristics of Unmodified F/A-18† and HARV*

Parameter	Unmodified	HARV
Weight (lbs)	31 980	35 765
Reference wing area (ft^2)	400	400
Reference MAC‡ (ft)	11.52	11.52
Reference Span (ft)	37.4	37.4
Center of Gravity (% MAC‡)	21.9	23.3
Roll inertia (slug-ft^2)	22 040	22 633
Pitch inertia (slug-ft^2)	124 554	174 246
Yaw inertia (slug-ft^2)	139 382	189 336
Product of inertia (slug-ft^2)	-2 039	-2 132
Overall length (ft)	56	56
Wing aspect ratio	3.5	3.5
Stabilator span (ft)	21.6	21.6
Stabilator area (ft^2)	88.26	86.48

† A Model F/A-18

* 60% fuel condition, landing gear up, clean configuration with pilot and support equipment

‡ Mean Aerodynamic Chord

Table 3. HARV Weights, Inertias, and Center of Gravity Locations

State	Weight (lbs)	X_{cg} (%MAC)	Z_{cg} (W.L.)	Ixx (slug-ft^2)	Iyy (slug-ft^2)	Izz (slug-ft^2)	Ixz (slug-ft^2)
Light	31 618	26.6	103.4	22 163	172 238	186 823	-2 043
Nominal	35 765	23.3	105.4	22 633	174 246	189 336	-2 132
Heavy	37 619	23.3	105.9	22 938	179 130	194 003	-2 507

Table 4. Lateral-Directional Design Flight Conditions

Angle-of-Attack (degrees)	Altitude (feet)	Load Factor (g's)	Weight*
5	25 000	1	Nominal
10	25 000	1	Nominal
15	25 000	1	Nominal
20	25 000	1	Nominal
25	25 000	1	Nominal
30	25 000	1	Nominal
35	25 000	1	Nominal
40	25 000	1	Nominal
45	25 000	1	Nominal
50	25 000	1	Nominal
55	25 000	1	Nominal
60	25 000	1	Nominal

* See Table 3

Table 5. Open-Loop Eigenvalues

Angle-of-Attack (degrees)	Spiral	Roll	Dutch roll frequency (rad/sec)	Dutch roll damping
5	.004	-1.4	1.67	0.12
10	.011	-.74	1.58	0.13
15	.006	-.46	1.56	0.12
20	-.033	-.28	1.77	0.09
25	-.019	-.24	1.77	0.10
30	-.055	-.20	1.25	0.28
35	-	(0.15 , 0.91)*	0.61	0.59
40	.151	-.36	0.41†	-1.17†
45	-.075	-.21	1.53	-0.09
50	-	(0.11 , 0.91)*	1.47	0.07
55	-	(0.09 , 0.90)*	1.51	0.10
60	-.036	-0.14	1.56	0.11

* Coupled roll-spiral mode (frequency , damping)

† Real dutch roll mode

Table 6. Lateral-Directional Evaluation Flight Conditions

Angle-of-Attack (degrees)	Altitude (feet)	Load Factor (g's)	Weight*
2.5	25 000	1	Nominal
5	15 000, 35 000	1	Nominal
10	15 000, 35 000	1	Nominal
15	15 000, 35 000	1	Nominal
20	15 000, 35 000	1	Nominal
25	15 000, 35 000	1	Nominal
30	15 000, 35 000	1	Nominal
35	15 000, 35 000	1	Nominal
40	15 000, 35 000	1	Nominal
45	15 000, 35 000	1	Nominal
50	15 000, 35 000	1	Nominal
55	15 000, 35 000	1	Nominal
60	15 000, 35 000	1	Nominal
65	25 000	1	Nominal
5	25 000	2, 4	Nominal
10	25 000	2, 4	Nominal
15	25 000	2, 4	Nominal
20	25 000	2, 4	Nominal
25	25 000	2, 4	Nominal
30	25 000	2, 4	Nominal
35	25 000	2, 4	Nominal
40	25 000	2, 4	Nominal
45	25 000	2, 4	Nominal
50	25 000	2, 4	Nominal
55	25 000	2, 4	Nominal
60	25 000	2, 4	Nominal
5	25 000	1	Heavy, Light
10	25 000	1	Heavy, Light
15	25 000	1	Heavy, Light
20	25 000	1	Heavy, Light
25	25 000	1	Heavy, Light
30	25 000	1	Heavy, Light
35	25 000	1	Heavy, Light
40	25 000	1	Heavy, Light
45	25 000	1	Heavy, Light
50	25 000	1	Heavy, Light
55	25 000	1	Heavy, Light
60	25 000	1	Heavy, Light

* See Table 3

Table 6. Concluded

Angle-of-Attack (degrees)	Altitude (feet)	Load Factor (g's)	Weight*
5	40 000	1	Heavy, Nominal, Light
10	40 000	1	Heavy, Nominal, Light
15	40 000	1	Heavy, Nominal, Light
20	40 000	1	Heavy, Nominal, Light
25	40 000	1	Heavy, Nominal, Light
30	40 000	1	Heavy, Nominal, Light
35	40 000	1	Heavy, Nominal, Light
40	40 000	1	Heavy, Nominal, Light
45	40 000	1	Heavy, Nominal, Light
50	40 000	1	Heavy, Nominal, Light
55	40 000	1	Heavy, Nominal, Light
60	40 000	1	Heavy, Nominal, Light

* See Table 3

Table 7. Desired Closed-Loop Design Eigenvalues

Angle-of-Attack (degrees)	Spiral	Roll	Dutch roll Frequency (rad/sec)	Dutch roll Damping
5	-.004	-2.2	1.6721	0.7
10	-.010	-2.0	1.5810	0.7
15	-.005	-1.9	1.5632	0.7
20	-.030	-2.2	1.7663	0.7
25	-.018	-2.1	1.7734	0.7
30	-.050	-1.4	1.2935	0.7
35	-.100	-1.0	1.00	0.7
40	-.100	-1.0	1.00	0.7
45	-.070	-0.7	1.5792	0.7
50	-.100	-0.7	1.4759	0.7
55	-.080	-0.7	1.5135	0.7
60	-.030	-0.7	1.5609	0.7

Table 8. Desired Eigenvectors

System States	Dutch Roll Mode (Magnitude, Phase(deg))	Roll Mode	Spiral Mode
Sideslip	(1 , 0)	0	0
Stability-axis Roll Rate	(x , x)	1	x
Stability-axis Yaw Rate	(x , x)	x	x
Bank Angle	(0 , 0)	x	1

x denotes elements not weighted in the cost function

Table 9. Lateral Stick and Pedals Shaping Functions

Pilot Input	Shape Function
Lateral Stick	Output=(1-0.4788*(1-0.3361*abs(input)))*0.3361*Input
Pedals	Output=0.01*(2.34838e-03*abs(Input)+0.763225)*Input

Table 10. Measurement Structural Filters†

Measurement	Numerator Frequency (rad/sec)	Numerator Damping	Denominator Frequency (rad/sec)	Denominator Damping
Stability-axis roll rate	80	0.08	80	0.7
Stability-axis yaw rate	150	0.08	150	0.7
Lateral acceleration	58	0.08	58	0.7
	80	0.08	80	0.7
Sideslip rate	80	0.08	80	0.7

† Filters have unity steady-state gain

Table 11. Lateral and Directional Feedback Gains

Lateral Feedback Gain Table†

Angle-of-Attack (degrees)	Stability-Axis Roll Rate Gain	Stability-Axis Yaw Rate Gain	Lateral Acceleration Gain	Sideslip Rate Gain
5	-0.6112	-0.7420	-0.0019	-0.3825
10	-1.3001	-0.9917	-0.1014	-0.1852
15	-1.5267	-0.8051	-0.0005	-0.6436
20	-2.0934	-1.4072	-0.6063	-1.2320
25	-2.2762	-1.1051	0.3622	-1.1257
30	-1.4900	-1.7434	0.1121	-1.2376
35	-1.1466	-1.9652	-0.2291	-0.9062
40	-1.0211	-1.3905	0.0175	-0.4289
45	-0.9574	-0.2758	-0.6353	-1.0400
50	-0.8741	-0.5382	-0.2759	-0.9231
55	-0.7826	-0.3339	-0.0765	-0.7941
60	-0.6847	0.0901	-0.3657	-0.1400

Directional Feedback Gain Table†

Angle-of-Attack (degrees)	Stability-Axis Roll Rate Gain	Stability-Axis Yaw Rate Gain	Lateral Acceleration Gain	Sideslip Rate Gain
5	-0.0524	0.1184	0.0524	1.7372
10	-0.0122	0.1826	0.0607	1.7539
15	0.0857	0.2316	0.0600	1.5931
20	0.2006	0.3522	0.2004	1.9451
25	0.2903	0.4131	0.0183	2.1152
30	0.1704	0.7166	-0.0254	1.6765
35	0.1384	0.7926	-1.3296	1.3411
40	-0.0608	0.4468	-2.0258	1.2669
45	0.3635	0.1073	-0.2938	1.5237
50	0.3420	0.3262	0.2016	1.3646
55	0.3158	0.3086	0.1557	1.5059
60	0.3007	0.1606	0.2077	1.3010

† Gains are for roll rate in (rad/sec), yaw rate in (rad/sec), lateral acceleration in (g's), and sideslip rate in (rad/sec)

Table 12. Acceleration Command Structural Filters*

Acceleration Command	Numerator Frequency (rad/sec)	Numerator Damping	Denominator Frequency (rad/sec)	Denominator Damping
Lateral	140	0.74	40	0.6
Directional	140	0.74	40	0.6

*Filters have unity steady-state gain

Table 13. Closed-Loop System Dutch Roll Cancellation

Angle-of-Attack (degrees)	$(\zeta_\phi \omega_\phi / \zeta_{dr} \omega_{dr})$	$(\omega_\phi / \omega_{dr})$
5	1.01	1.00
10	1.03	1.00
15	0.92	1.01
20	0.87	1.01
25	0.95	1.00
30	1.00	1.00
35	1.04	1.02
40	1.06	1.02
45	1.00	1.00
50	0.92	0.99
55	0.92	0.99
60	0.98	0.91

Table 14. Stability Margins for Variations of Stability Derivatives: Y_V, N_V, L_p, and N_r

Angle-of-Attack (degrees)	1g-15k ft $(\mu_R)^{-1}$/freq	1g-25k ft $(\mu_R)^{-1}$/freq	1g-35k ft $(\mu_R)^{-1}$/freq	2g-25k ft $(\mu_R)^{-1}$/freq	4g-25k ft $(\mu_R)^{-1}$/freq
5	3.99/0.52	4.25/0.52	4.22/0.52	4.57/0.52	
10	3.25/0.52	3.61/0.52	3.90/0.52	3.73/0.52	3.51/0.52
20	3.36/0.52	4.88/0.52	6.04/4.90	3.68/6.09	2.78/6.54
35	2.99/0.52	2.76/0.52	2.43/0.52	1.54/0.52	1.23/0.69
40	4.14/0.52	3.34/0.52	2.15/0.52	1.39/0.52	0.95/0.74
45	5.81/0.52	5.51/0.52	4.52/0.52	1.35/0.78	0.97/2.20
50	4.25/3.40	4.53/3.94	5.20/4.23		
55	3.85/3.66	4.53/3.94	4.86/4.23		

Frequency in units of radians/second

Table 15. Stability Margins for Variations of Control Derivatives: $L_{\delta ail}$, N_{rud}, $L_{\delta stab}$, and N_{yjet}

Angle-of-Attack (degrees)	1g-15k ft $(\mu_R)^{-1}$/freq	1g-25k ft $(\mu_R)^{-1}$/freq	1g-35k ft $(\mu_R)^{-1}$/freq	2g-25k ft $(\mu_R)^{-1}$/freq	4g-25k ft $(\mu_R)^{-1}$/freq
5	1.11/1.42	1.09/1.53	1.09/1.53	1.17/1.90	
10	1.04/1.23	1.01/1.23	.98/1.23	1.15/1.65	1.11/2.05
20	1.34/1.15	1.31/1.15	1.27/1.15	1.51/1.65	1.65/2.05
35	2.19/0.52	2.33/0.52	2.49/0.74	2.62/0.80	2.51/2.95
40	1.46/1.06	1.32/1.53	1.15/1.90	1.08/2.20	0.83/2.95
45	2.32/0.69	2.53/0.80	2.64/0.69	3.31/.92	3.14/6.54
50	2.87/0.60	2.73/0.64	2.62/0.52		
55	4.72/0.86	5.02/0.92	8.58/0.99		

Frequency in units of radians/second

Table 16. Lateral-Directional Coupling Guidelines

$\Delta\phi_w$	Maximum Excursion From Target Condition	
	$\Delta\alpha$	$\Delta\beta$
90°	±6°	7° adverse 1° proverse
90° ⇒ 360°	±10°	7° adverse 1° proverse

Table 17. Cooper-Harper Ratings from Five Pilots for all Maneuvers

Maneuver	Target	Pitch Rating†					Roll Rating†				
		P1	P2	P3	P4	P5	P1	P2	P3	P4	P5
1-g 360° roll with bank angle capture and α regulation from target α	$\alpha = 5°$	2	2	2	2	2	4.5	4	5	3	5
	$\alpha = 15°$	5	4	4	4	4.5	5	3	3	3	5
	$\alpha = 25°$	4	3	2.5	3	2.5	3	3	2.5	3	3
	$\alpha = 35°$	3	2	3	3	2	3	3	2.5	3	3
	$\alpha = 45°$	3	3	3	3	2	2	3	2.5	3	3
	$\alpha = 55°$	2.5	3	2.5	2	2	2	3	3	3	3
	$\alpha = 65°$	3	3	2.5	3	2	4	3	4	3	4.5
Loaded roll at M=0.6 with bank angle capture and α regulation	$\alpha = 5°$	3	2	2	2		4.5	4	5	3	5
	$\alpha = 15°$	4	3	4	3	3	4	4	5	3	3
	$\alpha = 25°$	3	3	4	3	3	3	3	4	3	3
Loaded roll at M=0.4 with bank angle capture and α regulation	$\alpha = 15°$	4	5	4	3	5	4	3	3	3	3
	$\alpha = 25°$	3	4	3	4	4.5	3	3	3	4	3
	$\alpha = 35°$	3	4	3	3	3	3	3	3	3	2
Target tracking M=0.6	3-g Target	3	5	4	4	5	2	4	3	3	4.5
Target tracking M=0.45	3-g Target	4	6	3	4	7	4	4	3	3	4.5
Lat./Dir. target acquisition	$\alpha = 30°$						5	5	4	4	6
Target tracking	$\alpha = 30°$	5	4	5	5	7	4	3	4	3	5.5
Lat./Dir. target acquisition	$\alpha = 45°$						5	5	4	4	7
Target tracking	$\alpha = 45°$	4.5	5.5	5	5	8	3	4	4.5	3	6

† Pi denotes rating from pilot number i

Table 18. Percentage of Ratings where CHR Spread was less than a Given Value

Difference between max. and min. CHR	Percent of ratings from 5 pilots	5 pilots minus 4 outlying points from 1 pilot
≤1	40%	46%
≤2	76%	84%
≤3	92%	100%
≤4	98%	-
≤5	100%	-

REPORT DOCUMENTATION PAGE

Form Approved
OMB No. 0704-0188

1. AGENCY USE ONLY (Leave blank)	2. REPORT DATE	3. REPORT TYPE AND DATES COVERED
	October 1998	Technical Publication

4. TITLE AND SUBTITLE
High-Alpha Research Vehicle Lateral-Directional Control Law Description, Analyses, and Simulation Results

5. FUNDING NUMBERS
WU 522-21-61-01

6. AUTHOR(S)
John B. Davidson, Patrick C. Murphy, Frederick J. Lallman, Keith D. Hoffler, and Barton J. Bacon

7. PERFORMING ORGANIZATION NAME(S) AND ADDRESS(ES)
NASA Langley Research Center
Hampton, VA 23681-2199

8. PERFORMING ORGANIZATION REPORT NUMBER
L-17673

9. SPONSORING/MONITORING AGENCY NAME(S) AND ADDRESS(ES)
National Aeronautics and Space Administration
Washington, DC 20546-0001

10. SPONSORING/MONITORING AGENCY REPORT NUMBER
NASA/TP-1998-208465

11. SUPPLEMENTARY NOTES
Davidson, Murphy, Lallman, Bacon: Langley Research Center, Hampton, VA;
Hoffler: ViGYAN Inc., Hampton,VA.

12a. DISTRIBUTION/AVAILABILITY STATEMENT
Unclassified-Unlimited
Subject Category 08 Distribution: Standard
Availability: NASA CASI (301) 621-0390

12b. DISTRIBUTION CODE

13. ABSTRACT (Maximum 200 words)
This report contains a description of a lateral-directional control law designed for the NASA High-Alpha Research Vehicle (HARV). The HARV is a F/A-18 aircraft modified to include a research flight computer, spin chute, and thrust-vectoring in the pitch and yaw axes. Two separate design tools, CRAFT and Pseudo Controls, were integrated to synthesize the lateral-directional control law. This report contains a description of the lateral-directional control law, analyses, and nonlinear simulation (batch and piloted) results. Linear analysis results include closed-loop eigenvalues, stability margins, robustness to changes in various plant parameters, and servo-elastic frequency responses. Step time responses from nonlinear batch simulation are presented and compared to design guidelines. Piloted simulation task scenarios, task guidelines, and pilot subjective ratings for the various maneuvers are discussed. Linear analysis shows that the control law meets the stability margin guidelines and is robust to stability and control parameter changes. Nonlinear batch simulation analysis shows the control law exhibits good performance and meets most of the design guidelines over the entire range of angle-of-attack. This control law (designated NASA-1A) was flight tested during the Summer of 1994 at NASA Dryden Flight Research Center.

14. SUBJECT TERMS
Lateral-Directional Control; High Angle-Of-Attack; Aircraft Control; CRAFT; Pseudo Controls; Feedback Control; HARV

15. NUMBER OF PAGES
72

16. PRICE CODE
A04

17. SECURITY CLASSIFICATION OF REPORT	18. SECURITY CLASSIFICATION OF THIS PAGE	19. SECURITY CLASSIFICATION OF ABSTRACT	20. LIMITATION OF ABSTRACT
Unclassified	Unclassified	Unclassified	